AGU PUBLICATIONS

Tectonics

RESEARCH ARTICLE
10.1002/2016TC004272

**Key Points:**
- New thermal and strength models of Mainland China are implemented
- Rheology controls the stability of tectonic structures
- Deep crust and mantle lithosphere in Tibet are week and prone to flow toward adjacent areas

**Supporting Information:**
- Supporting Information S1

**Correspondence to:**
Y. Deng, and M. Tesauro,
Yangfandeng@gig.ac.cn;
M.Tesauro@uu.nl

**Citation:**
Deng, Y., and M. Tesauro (2016), Lithospheric strength variations in Mainland China: Tectonic implications, *Tectonics*, *35*, 2313–2333 doi:10.1002/2016TC004272.

Received 10 JUN 2016
Accepted 12 SEP 2016
Accepted article online 14 SEP 2016
Published online 6 OCT 2016



# Lithospheric strength variations in Mainland China: Tectonic implications

**Yangfan Deng[1,2] and Magdala Tesauro[3]**

[1]State Key Laboratory of Isotope Geochemistry, Guangzhou Institute of Geochemistry, Chinese Academy of Sciences, Guangzhou, China, [2]State Key Laboratory of Lithospheric Evolution, Institute of Geology and Geophysics, Chinese Academy of Sciences, Beijing, China, [3]Department of Earth Sciences, Utrecht University, Utrecht, Netherlands

**Abstract** We present a new thermal and strength model for the lithosphere of Mainland China. To this purpose, we integrate a thermal model for the crust, using a 3-D steady state heat conduction equation, with estimates for the upper mantle thermal structure, obtained by inverting a *S* wave tomography model. With this new thermal model and assigning to the lithospheric layers a "soft" and "hard" rheology, respectively, we estimate integrated strength of the lithosphere. In the Ordos and the Sichuan basins, characterized by intermediate temperatures, strength is primarily concentrated in the crust, when the rheology is soft, and in both the crust and upper mantle, when the rheology is hard. In turn, the Tibetan Plateau and the Tarim basin have a weak and strong lithosphere mainly on account of their high and low temperatures, respectively. A comparison of temperatures, strength, and effective viscosity variations with earthquakes distribution and their seismic energy released indicates that both the deep part of the crust and the upper mantle of the Tibetan Plateau are weak and prone to flow toward adjacent areas. The high strength of some of the tectonic domains surrounding Tibet (Tarim, Ordos, and Sichuan basins) favors the flow toward the weak western part of South China block.

## 1. Introduction

The strength distribution in the continental lithosphere plays an essential role in controlling the behavior of continental deformation [e.g., *Ranalli and Adams*, 2013]. The present tectonics of Mainland China has been mainly affected by the Indo-Asian continental collision in the southwest, which has created the Tibetan Plateau, and the subduction of the NW Pacific plate in the east [e.g., *Pandey et al*., 2014]. Therefore, this region is obviously a key natural laboratory to investigate the influence that strength variations have on the evolution of intraplate continental lithosphere (Figure 1). In particular, the disruption of a part of its Archean cratons, due to the subsequent tectonic activity (see section 2), has attracted significant attention in the last decades [e.g., *Chen et al*., 2008, 2009; *Dong et al*., 2015]. Furthermore, numerous geophysical studies based on different observations, such as low seismic crustal velocities [*Yang et al*., 2012; *Deng et al*., 2015], seismic anisotropy [*Xie et al*., 2013], shear wave splitting measurements [e.g., *Li et al*., 2011], seismic attenuation distribution [e.g., *Zhao et al*., 2013], low electrical resistivity in the middle-lower crust [*Wei et al*., 2001; *Bai et al*., 2010], high $V_p/V_s$ ratio [e.g., *Singh et al*., 2015; *Xu et al*., 2014], and high heat flow [*Hu et al*., 2000] indicate a zone of strong viscosity reduction and partial melt beneath the Tibetan Plateau, which supports the hypothesis of flow of its crust/lithospheric mantle. However, the depth and extent of possible channels flow are still under debate. Some authors [e.g., *Clark and Royden*, 2000; *Klemperer*, 2006; *Royden et al*., 2008; *Wang et al*., 2012; *Xie et al*., 2013; *Jiang et al*., 2014] sustain the hypothesis that the flow primarily occurs within the middle-lower crust, based on the moderate amount of crustal shortening on the eastern plateau margin [*Burchfiel et al*., 1995]. Others [*Hirn et al*., 1995; *Huang et al*., 2008; *Wang et al*., 2008; *Liu et al*., 2004] suggest that the extrusion may occur widely in the asthenosphere.

On the other hand, the thermal structure and rheology of Mainland China has been investigated only in some parts of the region using heat flow and gravity data [e.g., *Jiménez-Munt et al*., 2008; *Zhang et al*., 2012, 2013a; *Robert et al*., 2015; *Tunini et al*., 2016]. In order to implement a consistent thermal and strength model for the whole Mainland China and identify the actual location of weak zones, where flow of crustal/lithospheric mantle rocks may be active, we estimate temperature, strength, and viscosity variations of the lithosphere of Mainland China, followed by an analysis of their relationship with intraplate seismicity distribution. To this purpose, we use the crustal temperatures model of *Sun et al*. [2013a] based on a 3-D steady state heat conduction equation, whereas we estimate upper mantle temperatures by inversion of the *S* wave velocity

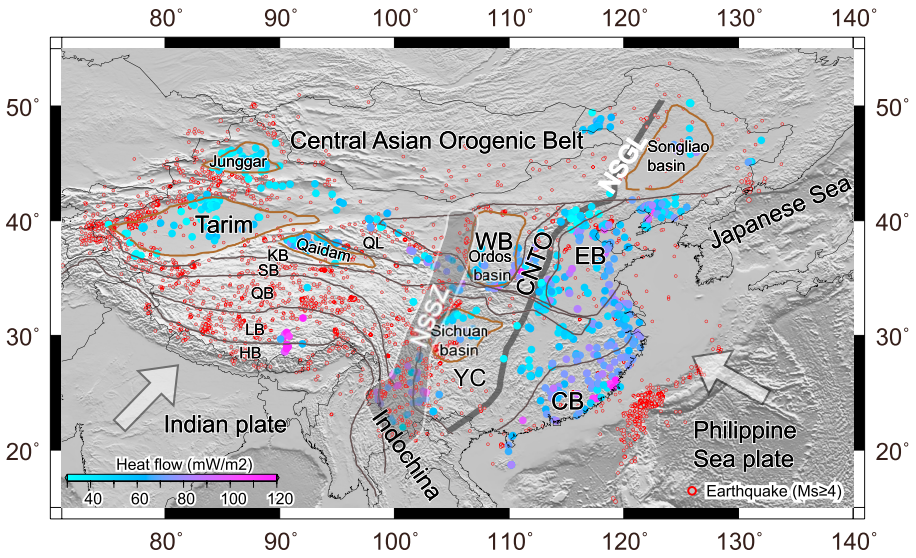


**Figure 1.** Topography and surface heat flow data of Mainland China (*Hu et al*., 2000; *Feng et al*., 2009). Red circles show the earthquakes ($M_s \geq 4$) occurring from 1980 to 2014 (China Earthquake Networks Center catalog). Grey and brown contours show main tectonic boundaries and the borders of the main sedimentary basins of Mainland China (Junggar, Tarim, Qaidam, Songliao, Ordos, and Sichuan basins). Abbreviations are as follows: HB: Himalayan block; LB: Lhasa block; QB: Qiangtang block; SB: Songpan-Ganzi block; KB: Kunlun-Qaidam block; QL: Qilian block; YC: Yangtze Craton; CB: Cathaysia block; NSGL: North-South Gravity Lineament; NSSZ: North-South seismic zone. The North China Craton is subdivided into a Western block (WB) and Eastern block (EB) by the Trans-North China Orogen (TNCO).

tomography data of *Li et al*. [2013]. We assume two end-members "hard" and "soft" rheology of the lithosphere to evaluate the influence of assumptions made in the rheological model on the overall strength distribution and in particular on the possible occurrence of channel flow at various depths of the lithosphere.

## 2. Geological Setting

Mainland China is an assembly of three major Precambrian cratons, the North China Craton (NCC) also called Sino-Korean Craton, the Yangtze Craton (YC), and the Tarim block, separated by fold belts, which were accreted from the late Proterozoic to the Cenozoic [e.g., *Zheng et al*., 2013; *Zhang et al*., 2014] (Figure 1).

The NCC is traversed by the North-South Gravity Lineament (NSGL), a large-scale feature 100 km wide, which extends over 3500 km in N-S direction. The eastern and western regions of the NCC have experienced very different geological histories. The regions located east to the NSGL underwent significant tectonic changes since the Jurassic and have been dominated by Cretaceous craton destruction [*Zhu et al*., 2011], leading to the removal of at least 100 km of its lowermost lithosphere [e.g., *Menzies et al*., 2007; *Xu*, 2007; *Chen et al*., 2008; *Windley et al*., 2010; *Dong et al*., 2015]. This has resulted in a thinned lithospheric mantle, an increase in heat flow, widespread volcanism, formation of large-scale sedimentary basins and extensive seismicity [e.g., *Griffin et al*., 1998; *Fan et al*., 2000; *Zheng et al*., 2007]. Different tectonic events have been proposed to be responsible for the decratonization of the eastern NCC. These include the India-Eurasia collision, mantle plume activity, collision of the NCC and YC cratons, and as the most likely the west Paleo-Pacific plate subduction [*Zhu et al*., 2012; *Zheng et al*., 2014]. Extensional tectonics induced by the Paleo-Pacific subduction had also significantly affected the lithosphere of the South China block, composed of the YC and Cathaysia block, causing widespread magmatism [*Li and Li*, 2007].

The western NCC was much less affected by Paleo-Pacific subduction, and thus, the lithosphere could preserve its thickness (up to >150 km) remaining mainly undeformed since the early Proterozoic (1.85 Ga) [e.g., *An and Shi*, 2006; *Chen et al*., 2009]. The northeastward subduction of the Indian continental plate at a rate of ~4 cm/yr [*Copley et al*., 2010] has significantly influenced the tectonics of this region, causing strong compressional deformation with crustal shortening and thickening. These processes induced the uplift of the Tibetan Plateau, east-west crustal extension inside the Plateau, and formation of several large active suture zones in and surrounding this region, where many large earthquakes have been generated [e.g.,

*Craig et al*., 2012]. The most active seismic region, as we can observe from the earthquakes distribution (Figure 1), is the North-South seismic zone (NSSZ), located along the eastern margin of the Tibetan Plateau and covering an area where several tectonic blocks, including the YC, the Songpan-Ganzi block, the Qiangtang block, and the Indochina block, are interacting.

## 3. Data and Methodology

### 3.1. Seismic Velocity Model

*P* and *S* velocity models of the upper mantle of the eastern part of Asia, based on tomography inversion of travel time [e.g., *Koulakov*, 2011; *Wei et al*., 2012] show relatively low seismic velocities, with high velocities up to a depth of 200 km or larger, beneath Precambrian blocks (e.g., Ordos basin, Sichuan basin, and Tarim basin). However, the vertical resolution of the body wave tomographic models is lower in comparison with that of surface wave models [e.g., *Li et al*., 2013]. In the last decade numerous surface wave tomography models could constrain absolute seismic wave velocities of the upper mantle of East Asia [e.g. *Feng et al*., 2010; *Zheng et al*., 2008; *Sun et al*., 2010]. These studies have detected the lateral variations of mantle structure in the different tectonic features but do not have sufficient resolution to resolve small-scale features ($<$500 km). *Li et al*. [2013] have recently presented a surface wave velocity model for the crust and upper mantle of East Asia, obtained by inverting Rayleigh wave group velocity data for periods between 10 and 145 s and combining the results with previously published Rayleigh wave phase velocity measurements between 150 and 250 s [e.g., *Koulakov*, 2011]. To estimate surface wave group velocities, *Li et al*. [2013] used waveform data recorded by permanent seismic stations recently installed in the study region, which have significantly improved the resolution of their tomography model.

The shear wave velocity model of *Li et al*. [2013] reveals significant heterogeneity in the upper mantle beneath China. It shows high-velocity anomalies up to a depth of 150–200 km beneath stable blocks, such as the Tarim Basin, West Yangtze Craton, Ordos basin, Indian continent, Southern edge of the Tibetan Plateau, and the Hindu Kush/Pamir region (Figure 2a). Beneath the Himalaya and Pamir regions high-velocity anomalies are present at a depth larger than 200 km and are associated with the subducting Indian plate. The low velocities observed beneath northern Tibet are indicative of a hotter upper mantle and are inconsistent with the interpretation of whole scale underthrusting of India beneath the entire Tibetan Plateau [*Zhou and Murphy*, 2005]. Other major low-velocity anomalies, indicating very thin lithosphere (70–100 km), occur beneath Eastern China and the marginal seas and correspond to areas of high heat flow, associated with Meso-Cenozoic extension and volcanism [e.g., *Wang and Cheng*, 2012].

### 3.2. Yield Strength Envelope

The bulk strength of the lithosphere is commonly described by the yield strength envelope (YSE) [*Goetze and Evans*, 1979], which predicts the maximum differential stress required to deform the rocks [*Ranalli*, 1995]. The YSE allows quantitative assessment of the lithospheric strength based on experimentally determined constitutive equations, describing brittle and ductile behaviors of rocks [e.g., *Brace and Kohlstedt*, 1980]. The brittle strength is described by Byerlee's law [*Byerlee*, 1978], while in the ductile regime, rocks deform according to power law dislocation creep at high stresses and temperature $<$1300°C (Table 1).

Notably, in the uppermost mantle at high stress and relatively low temperatures ($<$1000 °C), the ductile deformation occurs more likely according to the creep mechanism, known as "low-temperature plasticity" or "Dorn law" [e.g., *Ranalli and Adams*, 2013]. We refrain from using this flow law to estimate the lithospheric strength, since, differently from the power law dislocation creep, it has been derived only for olivine in anhydrous conditions [*Evans and Goetze,* 1979; *Mei et al*., 2010; *Demouchy et al*., 2013]. Thus, its application may not be suitable in the eastern part of the study area, characterized by metasomatized upper mantle.

The integrated lithospheric strength is obtained from the vertical integration of the yield strength envelope (1).

$$F_H = \int_0^H \mathrm{YSE} dz \tag{1}$$

where $H$ is the lithospheric thickness.

There is a large uncertainty in both assigning the rheology corresponding to a specific rock composition, which should be representative of the study area, as well as in the values of rheological parameters estimated

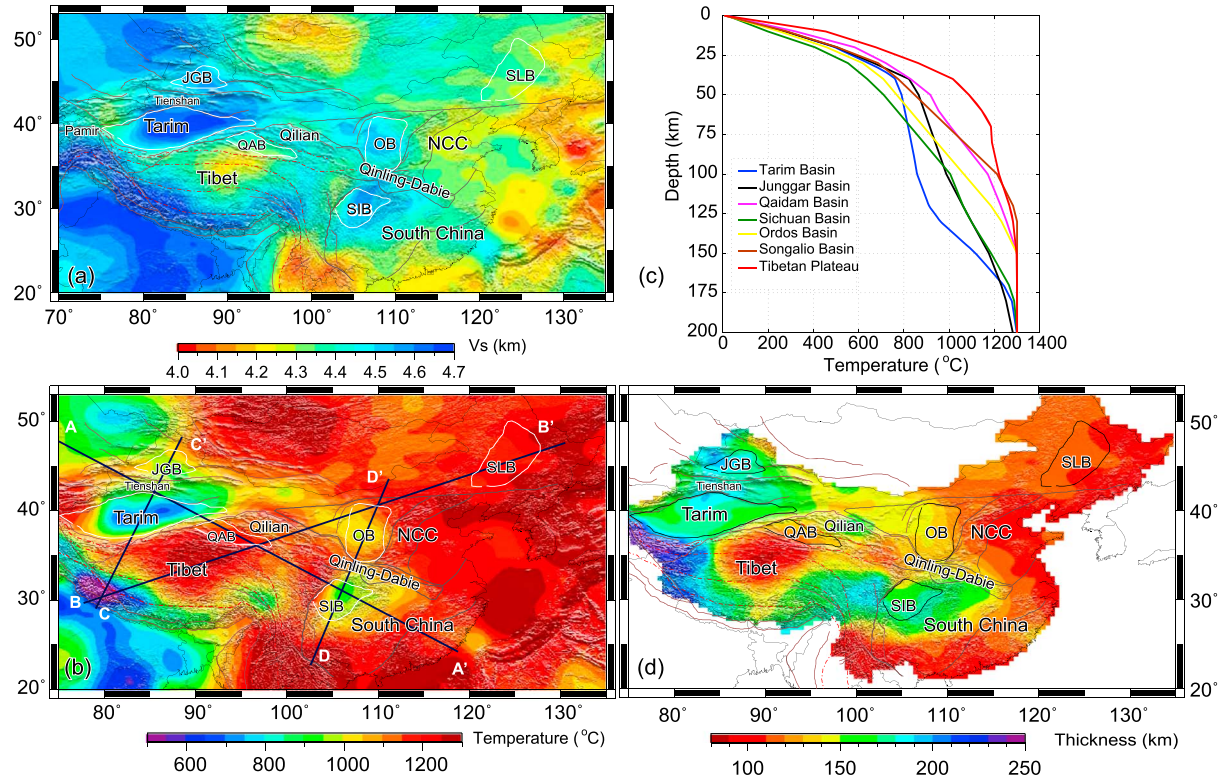


**Figure 2.** (a) Shear wave velocity (km/s) at a depth of 100 km [*Li et al.*, 2013]. (b) Temperature distribution (°C) in Mainland China at depths of 100 km. Black lines labeled A-A′, B-B′, C-C′, and D-D′ show location of four transects crossing Mainland China displayed in Figures 6–9. Abbreviations are as follows: JGB: Junggar basin; QAB: Qaidam basin; OB: Ordos basin; SIB: Sichuan basin; SLB: Songliao basin. (c) Average geotherms (°C) of some key tectonic structures. (d) Depth (km) of the thermal lithosphere corresponding to the depth of the 1250°C isotherm.

by laboratory experiments. For this reason, we construct two end-member lithospheric rheological models, here named soft and hard models, in order to estimate the strength of the lithosphere according to a weak and stiff rheology. In the soft model we assign a "wet quartzite," "wet diorite," "felsic granulite," and "wet peridotite" rheology to the upper crust, middle crust, lower crust, and upper mantle, respectively. In contrast, in

**Table 1.** Values of the Creep Parameters Assumed for Soft and Hard Rheological Models, Respectively

| Parameter | Symbol | Units | Sediments | Upper Crust | Middle Crust | Lower Crust | Upper Mantle |
|---|---|---|---|---|---|---|---|
| Composition | - | - | - | Quartzite (wet) [*Carter and Tsenn*, 1987]/quartzite (dry) [*Ranalli and Murphy*, 1987] | Diorite (wet) [*Carter and Tsenn*, 1987]/ diabase (dry) [*Kirby*, 1983] | Felsic-ganulite [*Wilks and Carter*, 1990]/ mafic-ganulite [*Wilks and Carter*, 1990] | Peridotite (wet) [*Hirth and Kohlstedt*, 1996]/ peridotite (dry) [*Hirth and Kohlstedt*, 1996] |
| Density min-max/mean | $\rho$ | $kg/m^{-3}$ | 1610–2290/2105 | 2400–2760/2711 | 2740–2860/2796 | 2850–3050/2945 | 3170–3450/3334 |
| Layer thickness min-max/mean | $z$ | km | 0–15.6/0.9 | 0.6/40.0/16.0 | 1.3–24.2/13.2 | 3.2–20.8/10.2 | - |
| Friction coefficient ext/com | $f$ | - | 0.75/3 | 0.75/3 | 0.75/3 | 0.75/3 | 0.75/3 |
| Pore fluid factor | $\lambda$ | - | 0.36 | 0.36 | 0.36 | 0.36 | 0.36 |
| Power law exponent | $n$ | - | - | 1.9/2.4 | 2.4/3.4 | 3.1/4.2 | 3.5/3.5 |
| Power law activation energy | $E_p$ | $kJ\ mol^{-1}$ | - | 172.6/156 | 212/260 | 243/445 | 515/535 |
| Power law pre-exponential stress constant | $A_p$ | $Pa^{-n}\ s^{-1}$ | - | $1.26\times10^{-13}$ /$2.508\times10^{-20}$ | $1.274\times10^{-16}$ /$7.962\times10^{-25}$ | $2.01\times10^{-21}$ /$8.83\times10^{-22}$ | $4.89\times10^{-15}$ /$4.85\times10^{-17}$ |
| Strain rate | $\dot{\varepsilon}$ | $s^{-1}$ | - | $10^{-15}$ | $10^{-15}$ | $10^{-15}$ | $10^{-15}$ |
| Brittle strength | $\sigma = f\rho gz(1-\lambda)$ | | | | | | |
| Power law creep | $\sigma = \left[\frac{\dot{\varepsilon}}{A_p}\right]^{\frac{1}{n}}.\exp\left[\frac{E_p}{nRT}\right]$ | | | | | | |

the hard model we associate to the same lithospheric layers a "dry granite," "dry diabase," "mafic granulite," and "dry peridotite" rheology. This choice implies that hydrated and sialic rocks are rheologically weaker than those anhydrous and mafic, as assessed by laboratory experiments [e.g., *Wilks and Carter*, 1990; *Hirth and Kohlstedt*, 1996]. The values of the creep parameters used for computation are given in Table 1.

For the strain rate (Table 1) we use a uniform value of $1\times10^{-15}\,s^{-1}$, which is commonly observed in most part of the study region [*Zhu and Shi*, 2011] and thus is suitable to estimate first-order strength variations. However, the strain rates may vary of about 2 orders of magnitude in the areas characterized by fast or slow deformation [e.g., *Kreemer et al*., 2014]. In particular, the horizontal strain rates of continental China, estimated using GPS observation, are about up to 5 times larger in the west than in the east [*Zhu and Shi*, 2011]. For this reason, we performed sensitivity tests of this parameter, by estimating the integrated strength for strain rates larger/lower than 1 order, with respect to the value used in this study. The depth of the intracrustal boundaries and density of the crustal layers are provided by the CRUST1.0 model [*Laske et al*., 2013], which estimates *Vp*, *Vs*, density and thickness for eight layers (water, ice, three sediment layers, and upper, middle, and lower crystalline crust) with a resolution of $1°\times1°$. The density of the upper mantle has been also provided by CRUST 1.0, which is taken from LLNL-G3Dv3 model [*Simmons et al*., 2012].

### 3.3. Thermal Model

The lithospheric thermal structure of continental China has been estimated in previous studies, following two different approaches: (1) solving the steady state thermal conduction equation, formulated in one or two dimension using heat flow data [e.g., *Zhang et al*., 2013a; *Chen et al*., 2014] and (2) inverting seismic velocity models [*An and Shi*, 2006; *Priestley and McKenzie*, 2006] using mineral physics constraints [*Cammarano et al*., 2003]. The results obtained, using the first approach, were influenced by the uneven distribution of the heat flow observations. *Sun et al*. [2013a] have recently estimated the thermal structure of the crust of Mainland China by solving the 3-D steady state heat conduction equation using a finite element method. They used the conductivity and heat production estimated from *P* wave velocities to fit the surface heat flow observations. The misfit found between the calculated and the observed surface heat flow resulted in an uncertainty of the estimated temperatures of $<100$°C. The model does not take into account the effect of local conditions, such as fluid circulation in the shallow part of the crust, which may bias these estimates [e.g., *Spinelli and Wang*, 2008]. In addition, a thermal model based on purely steady state conditions is in general not suitable for the upper mantle underlying tectonically active areas [e.g., *Mareschal and Jaupart*, 2013].

In contrast, inversion of seismic velocities into temperatures offers the advantage of having uniform data coverage and the opportunity to estimate the thermal field of the upper mantle also in tectonically active areas. As discussed previously [e.g., *Tesauro et al*., 2012, 2013, 2015], uncertainties in temperatures obtained from seismic inversion depend on various factors, and thus, the combined effects may be additive or subtractive, making a quantification difficult. The largest uncertainties are given by the seismic tomography model. An uncertainty in the seismic velocity of ~0.05 km/s may affect temperature more significantly (~150 °C) in the cold than in the warm regions, where velocity variations correspond to smaller temperature changes due to the anelasticity effect, a dissipative process involving viscous deformation [e.g., *Karato and Spetzler*, 1990].

We constructed a new composite model, by combining the thermal crustal model of *Sun et al*. [2013a] with estimates of temperatures in the upper mantle, obtained inverting seismic velocities of the shear model of *Li et al*. [2013] at a depth between 100 and 300 km. We linearly interpolate the temperatures estimated at a depth of 100 km with those at the Moho depth. The interpolation ensures a smooth transition between the crustal and upper mantle model. We use this "combined" approach to take advantage of both methods discussed, reducing the uncertainties of the estimated temperatures. Actually, the heat flow data reflect the thermal state of the crust. On the other hand, inversion of seismic velocities provides a valid alternative to estimate the upper mantle temperatures, enabling to identify features (e.g., presence of cold bodies in the upper mantle), which cannot be detected using the simple steady state thermal equation.

In the inversion, we apply the mineral physics approach of *Stixrude and Lithgow-Bertelloni* [2005], which consists of the evaluation of the physical properties of mantle phases at elevated pressure and temperature using the Eularian finite strain formulation. We used the elastic modulus and the pressure derivative of the mineral phases defined in *Cammarano et al*. [2003], which are estimated taking into account their dependence on the iron content. In the inversion we use a uniform upper mantle composition (Ol: 58.5%, OPX: 15%, CPX:11.5%, and Gt:15%, with a Mg# = 89), corresponding to an average of the mineral fractions constituting the

"Primitive mantle" rock defined by *McDonough and Sun* [1995] and the "Tecton garnet peridotite" rock of *Griffin et al*. [2003]. Using this composition we intend to represent both a "fertile" Phanerozoic upper mantle, which experienced a limited amount of melt extraction, as well as a Precambrian upper mantle, which has been refertilized by infiltration of fluids and partial melts. Presence of water and partial melt in the upper mantle may decrease significantly the seismic velocities [e.g., *Sato et al*., 1989], but their effects are not well constrained by experimental/theoretical results. As the presence of fluids enhances the effects of anelasticity, we take into account their influence on temperature by choosing the anelasticity model Q4 of *Cammarano et al*. [2003]. This model among others reproduces the anelasticity effect more strongly and thus simulates the effects of fluids on temperatures. Even if the uncertainties of the anelasticity may be large at high temperatures, they do not affect the strength estimates. Actually, the effects of anelasticity start to be activated at temperatures exceeding 900°C [e.g., *Jackson et al*., 2002], when the strength is already close to zero [e.g., *Ranalli,* 1994].

## 4. Lithospheric Temperature Distribution

The results of the new thermal model in terms of temperature variations at a depth of 100 km, average geotherms of some key tectonic stuctures, and depth of the thermal lithosphere are shown in Figures 2b−2d. We can observe that there is not everywhere a direct correspondence between the temperatures in the upper mantle and heat flow values (Figures 1 and 2). The most remarkable features, not reflected by the heat flow surface data, are the cold anomalies (500–600°C) along the southwesternern border of Tibet, caused by the subducting Indian slab. The temperatures sharply increase toward the central and northern part of the Tibetan Plateau (Qiangtang Terrane), reaching values close to the melting point (1100–1200°C). In this area the mean heat flow is also relatively high ($>75\ mW/m^2$) for a continental plate (Figure 1) and may have originated not only from the crust but also from the upper mantle. The average geotherm of central Tibet (Figure 2c) shows a high thermal gradient in the upper and middle crust, which lead to a temperature of ~1000°C at a depth of ~35 km. These results are consistent with those inferred from xenolith data (800° to 1000°C at a depths of 30 to 50 km) and satellite magnetic data (>550°C at depths of $15 \pm 5$ km) [*Hacker et al*., 2000]. At larger depths there is an abrupt strong reduction of the thermal gradient, which causes a very smooth increase of temperatures in the lower crust and in the upper mantle below 100 km and almost constant values (1200°C) at the depths 70–100 km. This trend shows that the uppermost part of the thickened Tibetan crust is warm, due to its high radiogenic heat production [e.g., *McKenzie and Priestley,* 2008] and the shear heating generated in the collisional setting [e.g., *Wang et al*., 2013a]. On the other hand, the subducting Indian plate is cooling the uppermost part of the Tibetan mantle and causes a marked change in the thermal gradient starting at the depth of the lower crust. Notably, the horizontal and vertical advection of material, associated with the relative motion between India and Tibet [*Craig et al*., 2012], as well as the anomalous heating of the middle crust, due to the radiogenic heat production [*Nunn et al*., 2014] or shear heating [*Wang et al*., 2013a], may cause a more severe decrease of the thermal gradient, which can lead to local temperature inversions, not captured by our model. Our results are also strongly consistent with those of *Jiménez-Munt et al*. [2008], predicting a temperature increase from the southern to the central and northern part of the Tibetan Plateau, according to the increase of distance from the Indian subducting slab. In the western part of China we identify a cold anomaly (~700°C), corresponding to a large part of the Tarim basin. We can observe that the thermal gradient in the mantle lithosphere of this basin is very low up to a depth of ~ 125 km and sharply increases below (Figure 2c). This transition can be attributed to a compositional variation between an uppermost mantle depleted of heavy constituents (e.g., garnet) and a fertile lower mantle lithosphere, accompanied by more hydrated conditions. This would demonstrate that the lithosphere of the Tarim basin has not been refertilized by metasomatism, like the eastern NCC. Since this basin is of Proterozoic age [*Zhang et al*., 2013b], we expect only a moderate depletion of its upper mantle [e.g., *Griffin et al*., 2003; *Tesauro et al*., 2014]. This would result in an underestimation of temperature in the shallow mantle of ≤100°C [*Tesauro et al*., 2014]. In contrast, the thermal gradient in the mantle lithosphere of the other basins is rather constant, showing only sharp discontinuities of very small amplitude (few tens of degrees), which indicate that compositional variations affecting the temperatures are not significant. The temperatures sharply increase of ~300°C in the westernmost part of the Tarim basin, reaching values up to ~1000°C beneath the Tien Shan orogen and the northern border of the Pamir region. The thermal anomaly underneath the Tien Shan orogen may be due to the upwelling of the asthenosphere below the

Asian plate [e.g., *Tian et al*., 2010]. This likely occurs as a consequence of the underthrusting of the Indian plate at a shallow angle to the north, which colliding with the Asian plate may cause bending and retreating of the subducted Asian mantle lithosphere to a deeper angle [*Kumar et al*., 2005].

The Tarim and Qaidam basins are characterized by a cold crust, according to their low heat flow estimates (Figure 1) and are underlain by a relatively cold and warm upper mantle, respectively (Figure 2c). These results indicate that the upper mantle of the Qaidam basin, differently from that of the Tarim basin, does not represent a strong rigid block. Other basins, located in the western and central part of China, as the Junngar, Ordos, and Sichuan basin, have similar intermediate temperatures at a depth of 100 km (~950°C), while at larger depths, the upper mantle of the Ordos basin is warmer than the others (Figures 2b and 2c). As also observed in previous studies [e.g., *Wang and Cheng,* 2012], the temperatures tend to smoothly increase eastwards reaching values close to the melting point (1100–1200°C) in the Trans-North China Orogen, South China fold belt, North China basin, and the Songliao basin. These tectonic structures are located in the parts of the craton that have been decratonized and subjected to strong extension during Meso-Cenozoic time. Previous studies [e.g., *Xu*, 2003; *Qiu et al*., 2006] have classified the continental basins located in the western (Ordos, Tarim, and Junggar basins) and eastern (Songliao basin) parts of China as "cold" and "hot" basins, respectively, on the base of the heat flow data. The last named show values near 70 mW/m$^2$ in the Songliao basin, NCC, and South China block (Figure 1). In contrast, in the western part of China the heat flow has much lower values, in the range between 35 and 45 mW/m$^2$ in the Junggar basin and 45–55 mW/m$^2$ in the Tarim basin (Figure 1). Our results demonstrate that this classification is too simplistic, since the temperatures in the upper mantle are more heterogeneously distributed, in comparison with the heat flow values. Therefore, we may identify the Tarim basin as a cold basin and the Songliao basin as a hot basin, while all the others are characterized by an intermediate thermal regime, with a geothermal gradient, which strongly decreases (as in the Sichuan and Junggar basin) or remains almost constant (as in the Qaidam and Ordos basins) at the Moho depth (Figure 2c).

The base of the thermal lithosphere corresponds to the depth of the mantle solidus temperature (i.e., 1300°C), at which the heat starts to be transferred by convection. Since the latter depends on mantle viscosity, which is also temperature dependent, the depth of the lithosphere/asthenosphere boundary may be shallower, corresponding to that of 0.85 of the solidus temperature [e.g., *Pollack and Chapman,* 1977]. In addition, mechanical properties of the mantle may change gradually in the vicinity of the solidus, making seismic velocities very sensitive to temperature variations near the melting point. Therefore, according to the thermal and seismological definition, the transition between the lithosphere and asthenosphere is smooth rather than sharp [e.g., *Cammarano et al*., 2003]. Due to the uncertainty in defining the depth of this boundary and considering also that the presence of fluids in the upper mantle decreases its solidus temperature, we assign as the base of the thermal lithosphere the depth of the 1250°C isotherm (Figure 2d). The thickest lithosphere (>200 km) is estimated along the southwestern part of Tibet. It appears that in this region the subducting Indian slab has doubled the thickness of the lithosphere. Large lithospheric thickness are also predicted in the study of *Tunini et al*. [2016], based on geological, geophysical, and petrological data. The lithosphere rapidly thins to 100–130 km in the central and northern part of the Tibetan Plateau and beneath the Qaidam basin, probably due to delamination processes [e.g., *Bao et al*., 2015] (Figure 2d). Similar variations of lithospheric thermal thickness have been estimated in the study of *Jiménez-Munt et al*. [2008]. These results suggest the removal of the lower part of the lithosphere with the consequent replacement with hotter asthenosphere in the central and northern part of the Plateau. In contrast, other studies based on seismic tomography [e.g., *Prestley et al*., 2006] and geoid anomalies, elevation data, and thermal analysis [*Robert et al*., 2015] suggest a very thick lithosphere (200–300 km) also in the northern part of the Tibetan Plateau.

Lithospheric roots extend to ~140 km depth beneath the Ordos block, to ~170 km depth beneath the Tarim and Sichuan basins, and to 200 km depth in the Junggar basin. These cratonic blocks, forming the northern and eastern borders of the Indian-Asian collision zone, have acted as rigid blocks affecting the lithospheric deformation around them during the collision [*Clark and Royden,* 2000; *Royden et al*., 2008]. These results are largely in agreement with those of *An and Shi* [2006] and *Li et al*. [2013], indicating that the seismological and thermal definition of the LAB is mostly coinciding. On the other hand, the model of *Tunini et al*. [2016] shows very similar temperature variations in the shallow lithospheric mantle (<150 km) of the Tarim and Junggar basins but predicts a lithospheric thickness larger than 200 km. In the eastern North China Craton

the lithosphere is 100–110 km, a value slighly larger than those previously predicted [e.g., *Chen et al*., 2008; *Yang et al*., 2013]. Thin lithosphere (~100 km) is also observed in the eastern part of South China block, indicating that extensional tectonics affected also this region.

## 5. Lithospheric Strength

Using the new thermal model presented above and assuming a soft and a hard rheological model of the lithosphere, we estimated the crustal and lithospheric integrated strength and the fraction of the integrated crustal strength for extensional and compressional stress conditions. The subduction processes in Western China caused compression of the lithosphere of the western portion in N-S direction, while the lithosphere of Eastern China entered into a stage of extension since the Cretaceous [e.g., *Zhang et al*., 2011a]. We display and discuss in this study only estimates of strength obtained for compressional stress conditions, which should be considered as upper bounds of the possible values depending on the local stress conditions (Figures 3a–3f).

It can be noticed that when a soft rheological model is used, most of the study area is weak, with an integrated lithospheric and crustal strength of $\sim 10^{12}$ Pa m (Figures 3a and 3c). The integrated lithospheric strength is relatively high in the eastern part of the continent ($\sim 1 \times 10^{13}$ Pa m), where the crustal thinning has the effect of increasing the strength in the mantle lithosphere. When we assume a hard rheology, the strength increases significantly ($> 1 \times 10^{13}$ Pa) in the lithosphere of several tectonic domains (Figures 3b and 3d). On the other hand, the Tibetan Plateau and the Qaidam and Junggar basins have a weak lithosphere, also when a hard rheology is assumed, on account of their high temperature and crustal thickness. We can notice that the choice of the rheology influences also the vertical strength partitioning between the lithospheric layers (Figures 3e and 3f). In case of a soft rheology, the strength is predominantly concentrated in the crust (>80%) in most of Mainland China, characterized by high or intermediate temperatures and a thick crust (>40 km). These areas deform according to a "crème brûlée" model, predicting a relatively strong crust underlaid by a weak mantle [e.g., *Jackson,* 2002]. In cold regions, as the Tarim basin or in those characterized by a relatively high thermal regime, but with a thin crust (<35 km), as part of Eastern China, the strength is almost equally partitioned between the crust and mantle lithosphere (Figure 3e). Therefore, these domains have a deformation type similar to that of a "jelly sandwich" model, in which the strength is distributed both in the crust and upper mantle [e.g., *Burov,* 2011]. When a hard rheology is assumed, the fraction of the strength concentrated in the crust is reduced to $\leq$40% in part of Eastern China and in the Tarim basin (Figure 3f). Therefore, the rheological stratification influences in some cases significantly the way in which the lithosphere deforms, on which in turn depends the long-term stability of the tectonic structures. Recent numerical models [*François et al*., 2013] demonstrate that the topography remains stable over geological time only when the strength is mainly concentrated in the mantle lithosphere. Therefore, by identifying the rheology that more likely represents the various tectonic structures and estimating their strength, we can make predictions on their long-term stability.

To analyze in more detail the strength distribution within the different lithospheric layers, we display some YSEs for key tectonic structures of Mainland China (Figure 4). We observe that in the Tibetan Plateau and northward in the Qaidam and Junggar basins the strength is localized only in the uppermost part of the crust, also when a hard rheology is used (Figure 4, YSE: B, G, and E). The absence of strength in the Lhasa and Qiangtang block may be related to partial melting of the middle/lower crust due to high temperatures, as suggested by the high values of the Poisson's ratio ($\geq$0.30 [*Singh et al*., 2015]). The heat causing partial melting derives probably from crustal thickening in the Lhasa block and from underplating of basaltic melts of mantle origin in the Qiangtang block [e.g., *Ji et al*., 2009]. Therefore, the high temperatures, causing the low rigidity of these domains, make them more prone to deformation and their high topography, supported by the hot upper mantle, unstable over geological time [e.g., *François et al*., 2013]. Similar to the Tibetan Plateau, the increase of strength in the Songliao basin, occurring by varying the rheology from soft to hard, is not significant (Figure 4, YSE D). Indeed, the high temperatures of the Songliao basin, formed during the late Jurassic and Cretaceous, when northeastern China experienced large-scale crustal extension and extensive volcanism, permit only a small concentration of the strength in the uppermost part of the mantle when a hard rheological model is assumed.

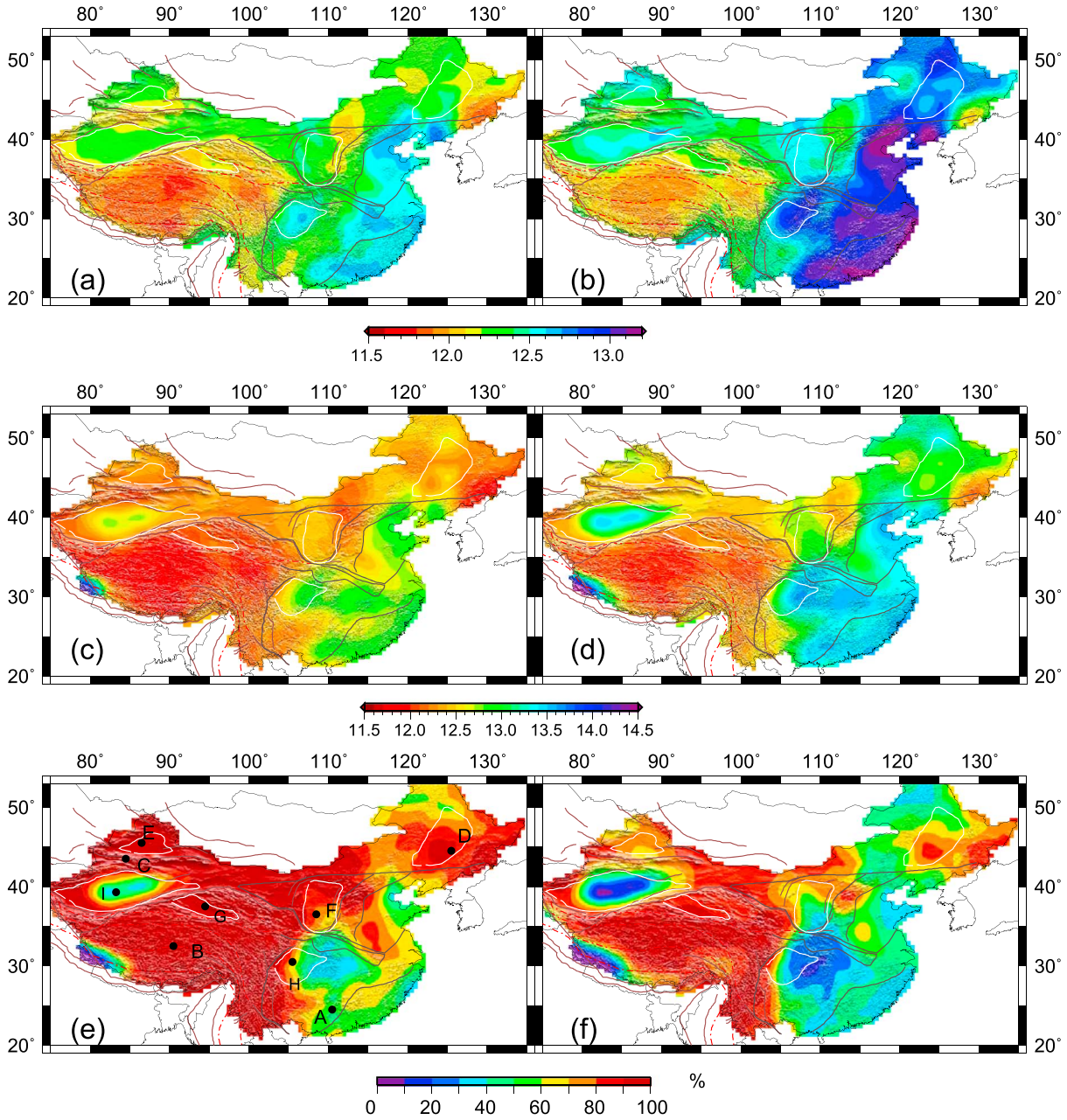


**Figure 3.** Integrated strength exponent of the (a, b) crust and (c, d) lithosphere and (e, f) percentage of integrated crustal strength, estimated assuming a soft (Figures 3a, 3c, and 3e) and a hard (Figures 3b, 3d, and 3f) rheological model, respectively. White contours delimit the sedimentary basins of Mainland China. Black dots, identified by capital letters (Figure 3e), show locations of YSEs displayed in Figure 4.

On the other hand, most of the Tarim basin and the YC have a strong upper mantle in both rheological models (Figure 4, YSE I and A). Therefore, also in this case, the choice of the rheology does not influence the strength distribution within these features, which corresponds to that of a jelly sandwich model. However, it should be noticed that the upper mantle of the Tarim basin increases significantly its strength, when a hard rheology is used. In the westernmost part of the Tarim basin, toward the Tien Shan orogen, the strength sharply decreases in both rheological models (Figure 4, YSE C), on account of the high temperatures (Figure 2b). Therefore, the high topography of the Tien Shan orogen is supported by the high temperatures of its upper mantle (responsible for its dynamic component) and by the rigid lithosphere of its foreland basin (Tarim basin), as already suggested in previous studies [e.g., *Kumar et al.*, 2005].

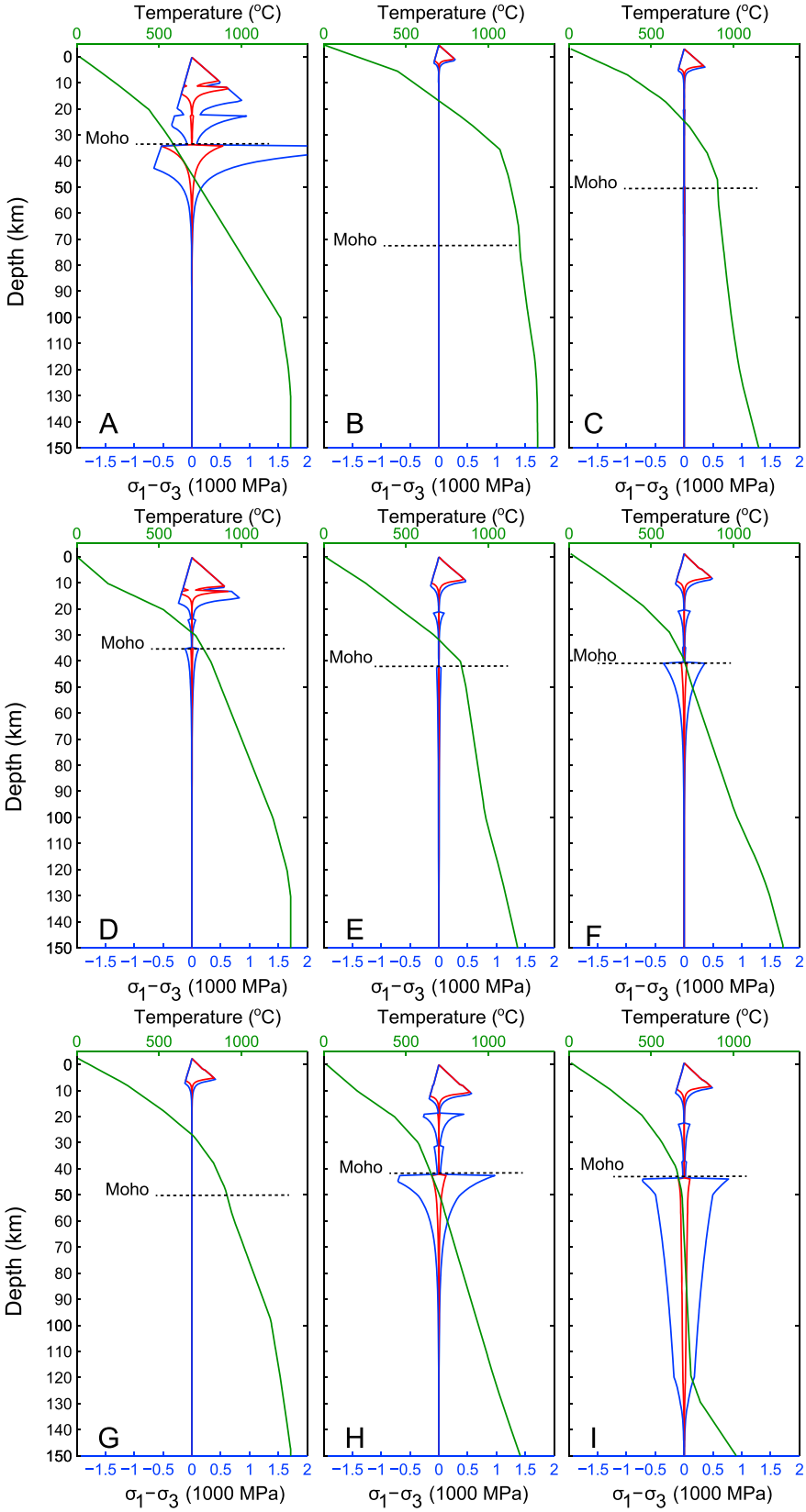


**Figure 4.** Geotherms (green contour) and YSEs of some key tectonic structures for a soft (red contour) and hard (blue contour) rheological model. Dashed black lines indicate depth of the Moho discontinuity. Locations of YSEs are displayed as black dots in Figure 3e.

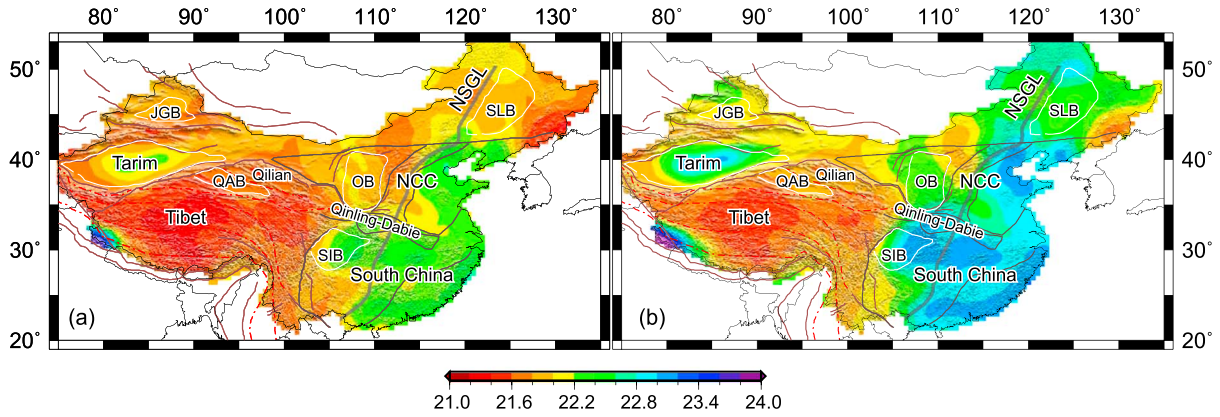


**Figure 5.** Exponent of vertically averaged effective viscosity ($\eta$) variations of the lithosphere, assuming (a) a soft and (b) a hard rheological model.

Other tectonic structures, located in the eastern part of continental China, as the Ordos and the Sichuan basins, deform according to a crème brûlée model, with the strength prevalently concentrated in the crust, when a soft rheological model is used, and according to a jelly sandwich model, with the strength distributed in all the lithospheric layers, when a hard rheology is assumed (Figure 4, YSE F and H). Therefore, in the latter case, these regions would represent strong rigid blocks hardly affected by the deformation of the cratonic lithosphere.

The results here presented show a first-order similarity with those of the global models of *Tesauro et al*. [2013], such as the difference between the strong Tarim basin and eastern part of Mainland China, with respect to the weak Tibetan Plateau. Such a difference is visible also in the global map of the effective elastic thickness (*Te*) of *Audet and Bürgmann* [2011], predicting values up to ~70 km in the Tarim basin and ~20 km in the Tibetan Plateau and surroundings. However, the strength variations between the different tectonic structures are in this study resolved in much more detail. We can further observe that the increase/decrease of the strain rates of 1 order of magnitude causes an increase/decrease of strength in the Tarim basin and the tectonic structures located in the eastern part of Mainland China, while there are almost no variations of strength in regions with a weak lithosphere as the Tibetan Plateau (supporting information Figure S1). These results confirm that the strain rate does not have a dominant effect on the strength distribution [e.g., *Tesauro et al*., 2015]. The uncertainties in temperature have also a variable impact on the strength estimates (supporting information Figure S2). Actually, an uncertainty of ±100°C in the mantle lithosphere has a negligible effect in regions with a high thermal regime as the Tibetan Plateau, where the Moho temperature is well above to the value at which the strength drops almost to zero (between 700°C and 900°C [*Ranalli*, 1994; *Burov and Diament*, 1995]). In contrast, in areas with a cold lithosphere, as the Tarim basin, the same uncertainty may significantly affect strength in the upper mantle.

## 6. Strength and Seismicity Relationship

In order to analyze the relationship between strength and seismicity distribution, we use the China Earthquake Networks Center (CENC) catalog to estimate along four transects the seismic energy released by earthquakes occurring in China between 1980 and 2014, with surface wave magnitude ($M_s$) ≥2.0, in comparison to the crustal integrated strength for the two end-members rheology (Figures 6a, 6b, 7a, 7b, 8a, 8b, 9a, 9b). The energy released by earthquakes is computed using the equation $\log E = 1.5 \times M_s + 11.8$ [*Gutenberg and Richter*, 1956; *Panza and Raykova*, 2008]. The value of $M_s$ is either taken directly from the CENC catalog or, when the event size is expressed as local ML magnitude in the CENC catalog, is calculated from currently available relationships between $M_s$ and ML, such as $M_s = 1.13 \times \mathrm{ML} - 1.08$ [*Fu and Liu*, 1980]. We also estimate the thickness of the seismogenic layer (*Ts*), which extends from the surface up to the depth above which 80% of the seismic energy is released. In addition, we plot along the same four transects the earthquakes with $M_s \geq 4.0$, together with temperatures and strength estimated for the two rheological models (Figures 6c–6e, 7c–7e, 8c–8e and 9c–9e).

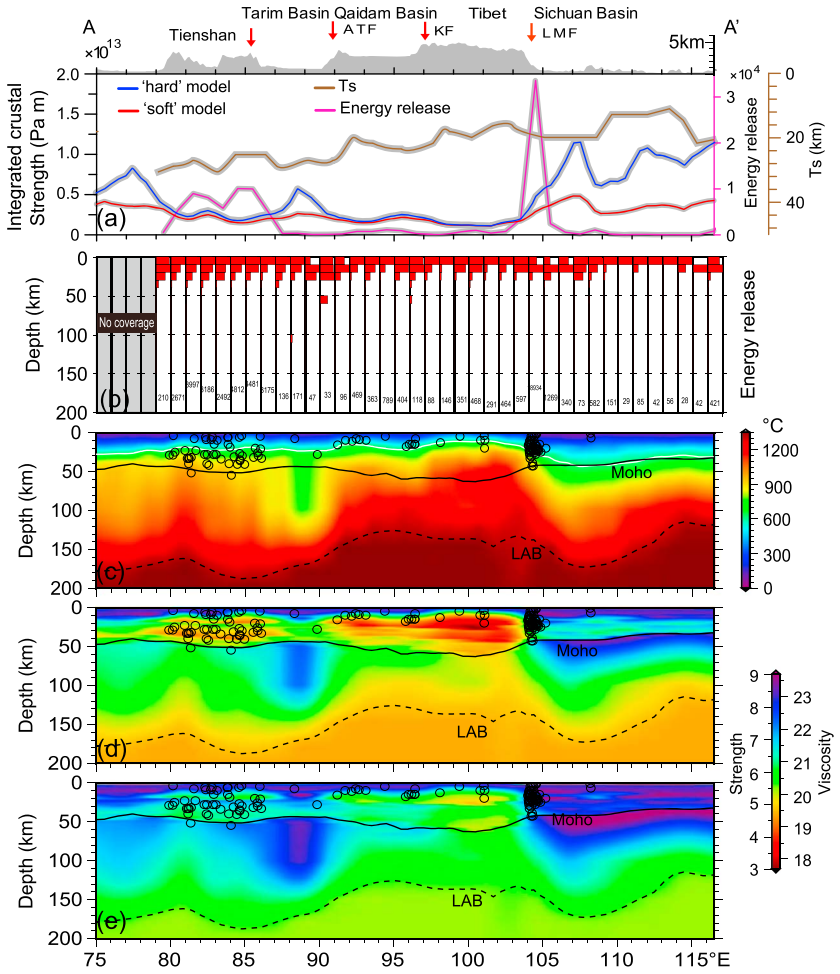


**Figure 6.** Transect A-A'; (a) Lateral variations of seismic energy, estimated for earthquakes ($M_s \geq 2$), seismogenic thickness (*Ts*, the seismogenic layer within which 80% of the seismic energy is released), and integrated crustal strength estimated for a soft and hard rheological models of lithosphere, respectively. Vertical red arrows indicate geographical location of main faults. Abbreviations stand as follows: ATF, AltynTagh fault; KF, Kunlun fault; LMF, Longmenshan fault. (b) Distribution of log $E/E_{max}$ versus depth. Numbers in each cell show the value for normalization (the maximum energy release within the depth interval) when the earthquakes are sorted in 10 km depth intervals. (c) Temperatures variations (°C). The white continuous line shows depth variations of the isotherm of 600°C. (d, e) Strength ($\sigma$) and effective viscosity ($\eta$) exponent variations, respectively, estimated for a soft and a hard rheological model. Black circles show locations of earthquake distribution ($M_s \geq 4$).

Notably, there is not a strict correlation between strength level and seismic energy release, since earthquakes do not occur above or below a predefined threshold of strength. However, the peaks of seismic energy are shifted with respect to those of integrated strength. This is because the largest energy release occurs in the areas characterized by sharp strength variations. A correlation between intraplate seismicity and pronounced changes of strength, in particular at cratonic edges, has been already suggested in previous studies [e.g., *Jiménez-Diaz et al.*, 2014; *Sloan et al.*, 2011; *Tesauro et al.*, 2014]. Seismicity appears generally to be restricted to the uppermost part of the crust up to a depth of ~20 km [e.g., *Maggi et al.*, 2000]. Therefore, earthquakes occur at a temperature 400°C (Figures 6c, 7c, 8c and 9c) above which most of the rocks composing the upper/middle crust (e.g., quartzite, granite, and diorite) are characterized by brittle behavior [e.g., *Ranalli,* 1995]. However, a large number of seismic events are located in the deep part of the crust (at a depth > 30 km) beneath the Tien Shan orogen (Figures 6a and 8a). The largest depth at which these seismic events occur corresponds to temperatures (600–700°C) at which most of the rocks undergo ductile deformation (Figures 6c and 8c). Therefore, the origin of this seismicity may be attributed to the presence of an anhydrous granulite-facies metamorphic assemblage, which can remain metastable and mechanically strong

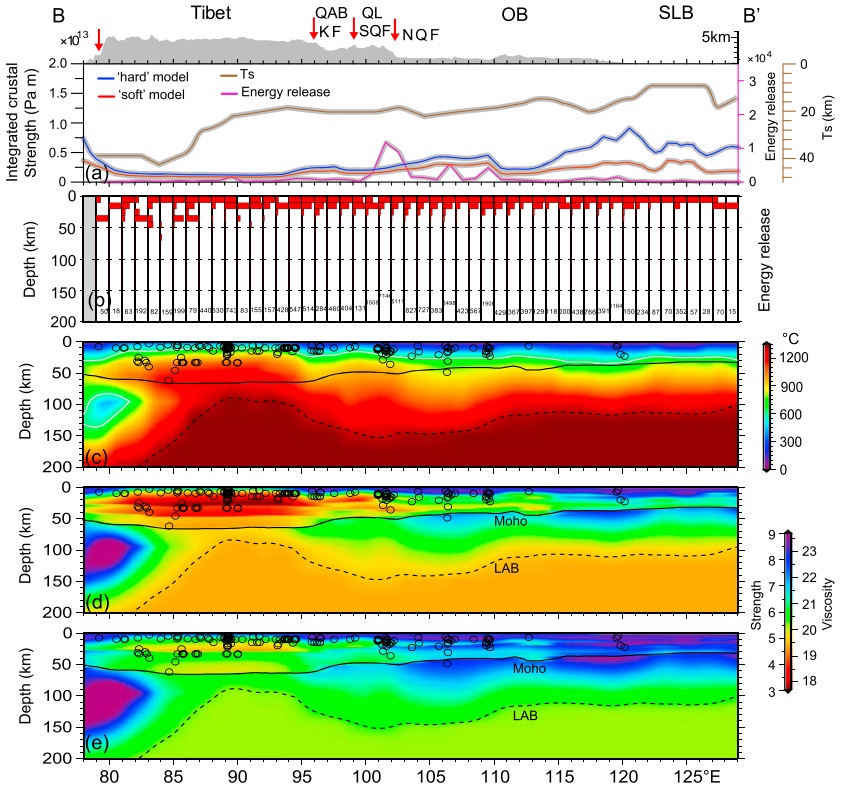


**Figure 7.** Transect B-B'. Features displayed are the same as in transect A-A'. Abbreviations are as follows: NQF, North Qilian fault; SQF, South Qilian fault. Other abbreviations are as in Figure 6.

[*Wang et al*., 1999; *Austrheim and Boundy,* 1994; *Lund et al*., 2004]. The hypothesis that these deep earthquakes occur as a result of brittle failure of dry mafic rocks is supported by the large amount of seismic energy released (up to $> 1 \times 10^4$) (Figures 6a and 8a).

We further observe in south Tibet some seismic events located in the middle crust (~35 km) or deeper, and thus, *Ts* in this area may be over 40 km (Figures 6a and 7a). At these depths our model predicts a temperature over 800°C (Figures 6c and 7c), at which the crustal rocks are in a ductile regime, as observed by the very low values of integrated strength in both rheological models used (Figures 6a, 7a, 8a, 6d, 6e, 7d, 7e, 8d, 8e). It should be noted that if a large number of earthquakes would occur under brittle failure conditions, existing because of the cooling induced by the subducting Indian slab [*Craig et al*., 2012], the seismic energy released would be likely much larger than that estimated ($<0.5 \times 10^4$, Figures 6a, 7a and 8a). We hypothesize that the fluids released by dehydration reactions in the subducting Indian slab may trigger the earthquakes generation, as already observed in other subduction environments, such as beneath the Molasse basin, the northern foreland basin of the Alps [*Deichmann,* 1992; *Sloan et al*., 2011].

## 7. Lateral Viscosity and Strength Variations

In order to identify the degree of stiffness of the different tectonic features of Mainland China, we have estimated the vertically averaged effective viscosity ($\eta$) of the lithosphere for both rheological models, calculated according to (2),

$$\eta = \frac{\Delta\sigma}{2\dot{\varepsilon}} \tag{2}$$

where $\Delta\sigma$ is the lithospheric strength. We can notice that in both rheological models there is a sharp contrast in $\eta$ between the tectonic features located west and east to the NSGL, which thus represents a lithospheric boundary (Figures 5a and 5b). Furthermore, the Tibetan Plateau is characterized by similar values of $\eta$ ($10^{21}$–$10^{22}$ Pa s) in both models, while the surrounding areas have an $\eta$ up to 2 orders larger. Such a variation in the rigidity of the lithosphere of Mainland China has been already noticed in previous studies by *England*

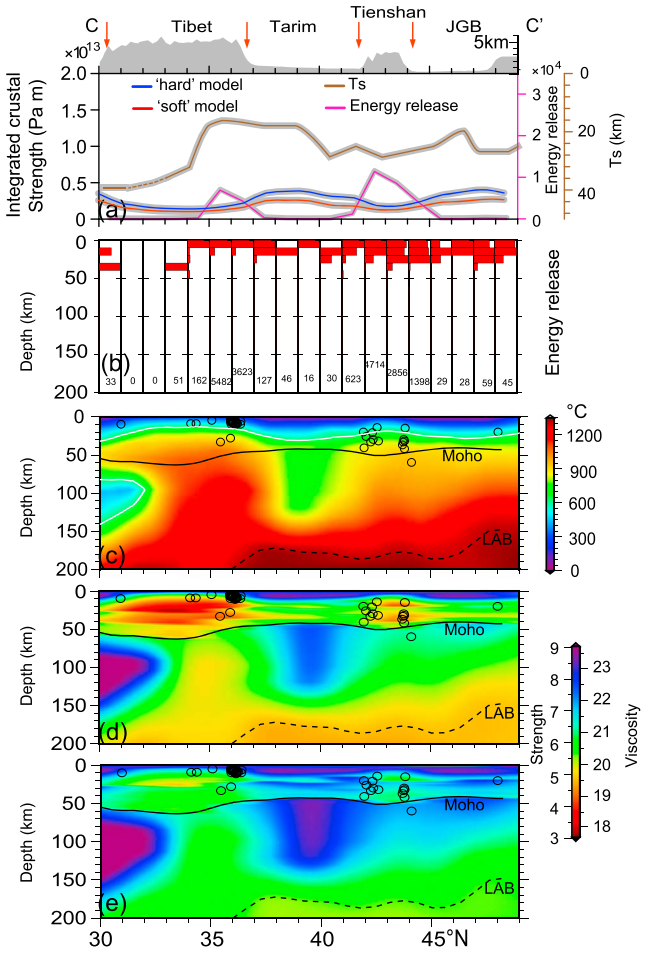


**Figure 8.** Transect C-C'. Features displayed are the same as in transect A-A'.

*and Molnar* [1997] and *Flesch et al.* [2001], which estimated $\eta$ based on a thin viscous sheet approach. Our estimates are in general half an order lower than those of *Flesch et al.* [2001]. This difference is within the uncertainties of the two approaches used. Differently from *Flesch et al.* [2001], in this study the minimum value of $\eta$ is in the central part of the Tibetan Plateau, where the temperatures are higher. In contrast, along its southwestern border, $\eta$ increases up to $10^{24}$ Pa s in the hard model, because of the high rigidity of the Indian subducting slab.

The difference between the two rheological models causes a variation of $\eta$ of less than 1 order and in particular is negligible in the Tibetan Plateau. This indicates that most of the Tibetan lithosphere, with a $\eta$ of only 10 or 100 times larger than the convecting upper mantle [e.g., *Billen and Hirth*, 2005], does not behave as a rigid plate, independently on the rheology assigned. Therefore, the use of a hard model implies an increase of the difference in the rigidity between Tibet and surrounding regions, such as the Tarim basin and Yangtze craton, where $\eta$ reaches values up to $\geq 10^{23}$ Pa s (Figure 5b). We also investigate the variation of strength ($\Delta\sigma$) and $\eta$, along the same four transects where we estimated the seismic energy variations (section 6). We can observe that in both rheological models the middle-lower crust and upper mantle of the Tibetan Plateau have negligible values of $\Delta\sigma$ ($\leq 10^6$ Pa), corresponding to a $\eta \leq 10^{20.5}$ Pa s (Figures 6d and 6e, 7d and 7e, and 8d and 8e); these values are consistent with those estimated in previous studies [*Sun et al.*, 2013b; *England et al.*, 2013]. These results predict in this area ductile deformation of both the middle-lower crust and mantle lithosphere [*Flesch et al.*, 2005], which may flow toward the adjacent regions. The deep part of the crust of the tectonic structures close to the Tibetan Plateau, as the Qaidam, Tarim, Ordos, and Sichuan basins, retain low $\Delta\sigma$ and $\eta$ ($<10^7$ Pa and $<10^{21.5}$ Pa s, respectively), when a soft rheological model is assumed. These low values indicate the presence of a thick (>20 km) zone of decoupling between the uppermost part of the crust and the mantle lithosphere (Figures 6d and 6e, 7d and 7e, 8d and 8e, and 9d and 9e). The decoupled zone progressively thins from SW to NE, reducing its thickness up to few kilometers beneath the Songliao basin (Figure 7d). These progressive increases of $\Delta\sigma$ are the direct effect of the decrease of the crustal thickness, which results in a decrease of the Moho temperature as well. In contrast, the uppermost part of the mantle underlying most of the regions surrounding the Tibetan Plateau retains an amount of $\Delta\sigma$ ($\geq 10^8$ Pa) and $\eta$ ($\geq 10^{22.5}$ Pa s) sufficient to prevent its flow (Figures 6d and 6e, 7d and 7e, 8d and 8e, and 9d and 9e). When a hard rheology is assumed, the increase of $\Delta\sigma$ and $\eta$ in the lower crust of the Tarim, Ordos, and Sichuan basins to values of ~$10^8$ Pa and ~$10^{22.5}$ Pa s, respectively, results in a strong reduction of the thickness of the ductile zone and a consequent coupling of their lithospheric layers. In addition, $\Delta\sigma$ and $\eta$ significantly increase in the upper mantle (~$10^9$ Pa and ~$10^{23.5}$ Pa s, respectively) up to a depth of ~ 150 km.

We can further notice that in both rheological models $\Delta\sigma$ tends to increase toward the center of the basins, where strong earthquakes are absent or located at a very shallow depth, as beneath the Qaidam basin

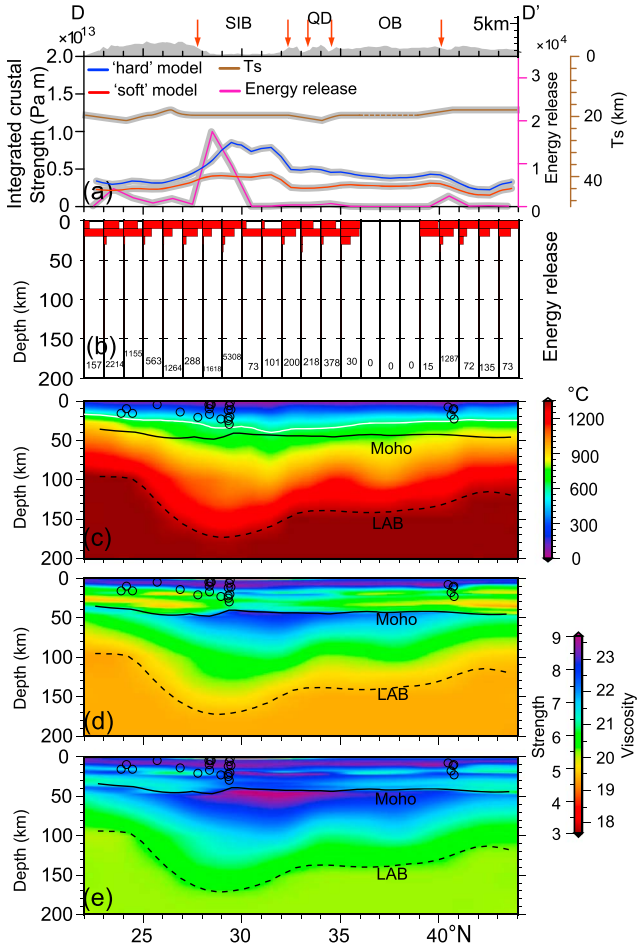


**Figure 9.** Transect D-D'. Features displayed are the same as in transect A-A'. Abbreviations are as follows: QD: Qinling-Dabie orogen. Other abbreviations are as in Figure 6.

(Figures 6–9). Consequently, the seismic energy, which is large in correspondence to the main faults boarding the basins ($2\times10^4$), significantly drops toward their centers (Figures 6a and 9a).

In this regard, we speculate that the crustal rheology of these basins is sufficiently strong to prevent brittle failure. This hypothesis is supported by seismic data which predict, values of crustal velocities (up to 7.1 km/s in the lower crust) and Poisson's ratio (0.26–0.29) indicating an intermediate (in the Qaidam, Sichuan, and Ordos basins) or mafic (in the Tarim basin) crustal composition [e.g., *Zhang et al.*, 2010, 2011b; *Wang et al.*, 2013b; *Zhao et al.*, 2013]. Furthermore, velocity models, viscosity structure deduced from the postseismic deformation, magnetotelluric data, and geodynamic models indicate a strong contrast in lithospheric rheology between Tibet and the Tarim, Ordos, and Sichuan basins [e.g., *Li et al.*, 2013; *Sun et al.*, 2013b, 2014; *Huang et al.*, 2014; *Bao et al.*, 2015]. On the base of these inferences, it appears that a hard more than a soft rheology represents the lithospheric structure of these basins, which are considered remnants of old cratons, remained undeformed during the orogenic events that formed the Tibetan Plateau [e.g., *Zhao et al.*, 2013]. Therefore, considering the hard rheological model more realistic, the rigid lithosphere of these basins would provide an obstacle to the flow of the Tibetan lower crust, diverting it toward regions of weaker lithosphere.

On the other hand, the lower crust and mantle lithosphere of the Qaidam basin have values of $\Delta\sigma$ ($<10^7$ Pa) and $\eta$ of ($<10^{21.5}$ Pa s), respectively, and thus remain weak also when we assume a hard rheology. Such a weakness may promote the flow of the Tibetan lower crust/mantle lithosphere beneath this basin. This hypothesis is supported by the low resistivity estimated from magnetotelluric experiments [*Xiao et al.*, 2013; *Wei et al.*, 2014], wide angle seismic data [*Karplus et al.*, 2011], and ambient noise tomography [e.g., *Karplus et al.*, 2013]. South to the Sichuan basin, between the southern part of the YC and the Cathaysia block, we can observe a progressive thinning of the thermal lithosphere (Figure 2d) and a decrease of $\Delta\sigma$ (Figures 6d and 6e), which would cause the flow of the Tibetan lower crust/lithospheric mantle in this direction, as already suggested in previous studies [*Li et al.*, 2008; *Royden et al.*, 2008]. The formation of a channel flow south of the Sichuan basin would be favored in case the lithosphere of this region has a soft rheology. This hypothesis is supported by the moderate values of Poisson's ratio of the crust of the South China block, which suggest the dominance of felsic composition in the crust [e.g., *Ji et al.*, 2009] and by GPS velocities and *SKS* wave splitting vectors. These data indicate that the deformation in the Tibetan Plateau starts between its central and western part, moves clockwise around the Eastern Himalaya, and ends at the southeast corner of the plateau with a fan-like front [*Gan et al.*, 2007; *Chen et al.*, 2015]. We can also notice that this area is seismically active, but the earthquakes, and thus the deformation occurring in a brittle condition, are limited to the shallow upper crust. In contrast, the lithosphere of the eastern part of the Qinling orogen, between the Ordos and Sichuan basins, does not show any significant variation in terms of thickness and $\Delta\sigma$, in

comparison with that underlying the two basins (Figures 9d and 9e). Notably, this area is almost aseismic, as also shown by the negligible amount of the seismic energy released (Figure 9a). Therefore, our models do not support a crustal rheology of the Qinling orogen weaker than that characterizing the two adjacent basins, which would favor the flow of the Tibetan lower crust/lithospheric mantle toward this area, as predicted by previous studies [e.g., *Enkelmann et al.*, 2006; *Huang et al.*, 2008; *Zhang et al.*, 2012]. Low values of $V_p/V_s$ ratios in the Qinling orogen [*Wang et al.*, 2014] and high velocity in its western part [*Li et al.*, 2014] are also not consistent with the flow of significant amounts of crustal material between the Ordos and the Sichuan stable blocks.

## 8. Conclusions

We have presented a new thermal and strength/viscosity model of the lithosphere of Mainland China. The temperatures in the upper mantle, at a depth of 100 km, span from ~700°C in the Tarim basin to over 1100°C in Tibet and in the eastern part of Mainland China, which has been affected by strong extension since the Mesozoic. The depth of the thermal lithosphere, estimated as the depth of the 1250°C isotherm, varies significantly beneath the Tibetan Plateau, ranging between $>200$ km in its southwestern part, due to the effect of the subducting Indian slab, and $<130$ km in its central and northern part. In other regions of Mainland China as the Tarim, Sichuan, and Ordos basin, the lithospheric thickness is relatively large, spanning between 140 km and 170 km, while it thins in Eastern China to ~100 km, due to the disruption of the cratonic lithosphere.

In the regions characterized by low (e.g., Tarim basin) and high temperatures (e.g., Tibetan Plateau), the lithospheric strength and viscosity is not significantly affected by the rheological type assigned, being in both rheological models distributed in the crust and upper mantle or dominantly concentrated in the uppermost part of the crust. In contrast, the rheology influences remarkably the strength and viscosity distribution between the lithospheric layers, and thus the long-term stability of the tectonic structures, with an intermediate thermal regime (e.g., the Ordos and Sichuan basins).

The Tibetan Plateau has a lithospheric vertically averaged effective viscosity 1 or 2 orders lower than the surrounding tectonic features (~$10^{21}$ Pa s). Its weak lower crust and mantle lithosphere are prone to flow toward the adjacent areas. However, the large lithospheric strength of the Tarim, Ordos, and Sichuan basins, enhanced by their hard rheology, reduces significantly this material extrusion.

Deep earthquakes releasing high seismic energy ($>1\times10^4$) occur beneath Tien Shan and are correlated with sharp lateral strength variations. In contrast, the seismic energy released by the earthquakes located at deeper levels of the crust of south Tibet, is much lower ($<0.5\times10^4$).

## Appendix A: Mineral Physics Approach

To invert the seismic velocity in temperature, we estimate the anharmonic velocity of a peridotite containing four main mineral phases (Ol, OPX, CPX, and Gt). Each one is treated as an ideal solid solution of *Mg* and *Fe* species (end-members) and in case of Gt also of *Ca* species (end-member): Ol (forsterite + fayalite), OPX (enstatite + ferrosilite), CPX (diopside + hedenbergite), and Gt (pyrope + almandine + glossular). The bulk and the shear modulus ($K_0$ and $G_0$) and the pressure derivative of each mineral phase at zero pressure ($P_0$) and room temperature ($T_0 = 300$ K) (STP conditions) are taken from *Cammarano et al.* [2003]. All the other parameters displayed in the equations below of each end-member at the same STP conditions are taken from *Stixrude and Lithgow-Bertelloni* [2005].

To estimate the bulk and shear modulus of each mineral phase as a function of temperature and pressure, we express the total pressure, $P_{TOT}(V,T)$, as a sum of the pressure at reference temperature, $P_{ref}$ (e.g., isothermal compression at 300 K), and the thermal pressure, which increases along an isochore, $\Delta P_{th}$:

$$P_{TOT}(V,T) = P_{ref}(V) + \Delta P_{th}(V,T) \tag{A1}$$

Isothermal compression is estimated through the third-order Birch-Murnaghan equation:

$$P_{st} = \frac{3}{2}K_{T_0}\left[\left(\frac{V_0}{V}\right)^{\frac{7}{3}} - \left(\frac{V_0}{V}\right)^{\frac{5}{3}}\right]\left\{1 - \frac{3}{4}\left(4 - K'_{T_0}\right)\left[\left(\frac{V_0}{V}\right)^{\frac{2}{3}} - 1\right]\right\} \tag{A2}$$

where $V$ is the molar volume at the temperature considered ($T$). The thermal pressure can be described using the Debye model [*Jackson and Rigden*, 1996]:

$$\Delta P_{\mathrm{th}} = \frac{\gamma(V)}{V}\left[E_{\mathrm{th}}(V,T) - E_{\mathrm{th}}(V,T_0)\right] \tag{A3}$$

where $\gamma$ is the Grüneisen parameter, which describes the effect that changing the volume of a crystal lattice has on its vibrational properties, and, as a consequence, the effect that changing temperature has on the size or dynamics of the lattice. It is assumed to have the form

$$\gamma = \gamma_0\left(\frac{V}{V_0}\right)^q \tag{A4}$$

where $q$ is the volume dependence of the Grüneisen parameter ($q = \mathrm{d}\ln\gamma/\mathrm{d}\ln V$), which is assumed to be constant for each end-member [*Stixrude and Lithgow-Bertelloni*, 2005].

$E_{\mathrm{th}}$ is the vibrational energy for a given volume and temperature, which can be calculated from the Debye model:

$$E_{\mathrm{th}} = \frac{9nRT}{(\theta/T)^3}\int_0^{\theta/T}\frac{x^3\mathrm{d}x}{e^x - 1} \tag{A5}$$

where $\frac{3}{(\theta/T)^3}\int_0^{\theta/T}\frac{x^3\mathrm{d}x}{e^x-1}$ is the Debye function (with $\theta$ the Debye temperature (A10)), $R$ the gas constant, and $n$ the number of atoms per formula unit.

The isentropic bulk modulus as function of temperature and pressure, corrected for the difference between isothermal and isentropic values, is given by

$$K = K_T(1 + \alpha\gamma T) \tag{A6}$$

where $\alpha$, the thermal expansion coefficient, is

$$\alpha = \gamma C_v / K_T V \tag{A7}$$

and $K_T$ is

$$\begin{aligned} K_T(V,T) = {} & K_0(1+2f)^{5/2}\left[1 + \left(3K_0' - 5\right)f + 27/2\left(K_0' - 4\right)f^2\right] \\ & + \left({}^{\gamma}/_{V}\right)(\gamma + 1 - q)E_{\mathrm{th}}(V,T) - E_{\mathrm{th}}(V,T_0) - \left({}^{\gamma^2}/_{V}\right)\left(TC_{v(V,T)} - 300C_{v(V,300k)}\right) \end{aligned} \tag{A8}$$

which agrees with the expression to third order derived from a purely isotropic thermodynamic analysis [*Stixrude and Lithgow-Bertelloni*, 2005].

In (A7) and (A8) $Cv$ is the heat capacity at constant volume:

$$C_v = \left({}^{\mathrm{d}}E_{\mathrm{th}}/_{\mathrm{d}}T\right)_v = {}^4E_{\mathrm{th}}/_T - 9nR\left({}^{\theta}/_{T}\right)/\left[\exp\left({}^{\theta}/_{T}\right) - 1\right] \tag{A9}$$

where $\theta$, the Debye temperature, is estimated as

$$\theta = \theta_0 \mathrm{Exp}\left(\frac{\gamma_0 - \gamma(V)}{q}\right) \tag{A10}$$

In (A8) $K_0'$ is the pressure derivative of the bulk modulus $K_0$ and $f$ is

$$f = \frac{1}{2}\left[\left(\frac{V_0}{V}\right)^{2/3} - 1\right] \tag{A11}$$

The shear modulus as a function of temperature and pressure is given by

$$\begin{aligned} G(V,T) = {} & (1+2f)^{5/2}\left[G_0 + \left(3K_0G_0' - 5G_0\right)f + \left(6K_0G_0' - 24K_0 - 14G_0 + \frac{9}{2}K_0K_0'\right)f^2\right] \\ & - \eta_s\frac{E_{\mathrm{th}}(V,T) - E_{\mathrm{th}}(V,T_0)}{V} \end{aligned} \tag{A12}$$

where $G_0^{'}$ is the pressure derivative of the shear modulus $G_0$ and $\eta$ is the shear strain derivative of $\gamma$ [*Stixrude and Lithgow-Bertelloni,* 2005].

$$\eta_s = \eta_{s0}\left(\frac{V}{V_0}\right) \tag{A13}$$

The density as a function of temperature and pressure is estimated dividing the molar mass ($m$) by the molar volume ($V$):

$$\rho = \left(\frac{m}{V}\right) \tag{A14}$$

Once we estimated the anharmonic velocities of the peridotite, we applied the anelastic correction using an attenuation model (in this study Q4 from *Cammarano et al*. [2003]).

**Acknowledgments**

We are very grateful to Yonghua Li of the Institute of Geophysics, Chinese Earthquake Administration, for providing us its seismic velocity model and to Yujun Sun of the Institute of Geomechanics, Chinese Academy of Geological Sciences, for providing us the crustal temperature model. We are grateful to Sierd Cloetingh for constructive suggestions on an early version of this manuscript. We thank Jose Badal, Jing Wu, Lin Chen, and Xinlei Sun for valuable discussions and suggestions. We acknowledge the China Earthquake Networks Center (CENC), for compiling the seismicity data. This research was funded by the Strategic Priority Research Program (B) of the Chinese Academy of Sciences (grant XDB18030101), the National Science Foundation of China (grant 41504069), Utrecht University, and the Netherlands Research Centre for Integrated Solid Earth (ISES-2014-UU-08 and ISES-2016-UU-19). The data used in this paper are available upon request from the corresponding author (yangfandeng@gig.ac.cn). Constructive comments of two anonymous reviewers have greatly improved the manuscript.

## References

An, M., and Y. Shi (2006), Lithospheric thickness of the Chinese continent, *Phys. Earth Planet. Inter.*, *159*(3-4), 257–266.

Audet, P., and R. Bürgmann (2011), Dominant role of tectonic inheritance in supercontinent cycles, *Nat. Geosci.*, *4*, 184–187.

Austrheim, H., and T. Boundy (1994), Pseudotachylytes generated during seismic faulting and eclogitization of the deep crust, *Science*, *265*(5168), 82–83.

Bai, D., M. J. Unsworth, M. A. Meju, X. Ma, J. Teng, X. Kong, Y. Sun, J. Sun, L. Wang, and C. Jiang (2010), Crustal deformation of the eastern Tibetan Plateau revealed by magnetotelluric imaging, *Nat. Geosci.*, *3*(5), 358–362.

Bao, X., X. Song, and J. Li (2015), High-resolution lithospheric structure beneath Mainland China from ambient noise and earthquake surface-wave tomography, *Earth Planet. Sci. Lett.*, *417*, 132–141.

Billen, M. I., and G. Hirth (2005), Newtonian versus non-Newtonian upper mantle viscosity: Implications for subduction initiation, *Geophys. Res. Lett.*, *32*, L19304, doi:10.1029/2005GL023457.

Brace, W., and D. Kohlstedt (1980), Limits on lithospheric stress imposed by laboratory experiments, *J. Geophys. Res.*, *85*, 6248–6252, doi:10.1029/JB085iB11p06248.

Burchfiel, B., C. Zhiliang, L. Yupinc, and L. Royden (1995), Tectonics of the Longmen Shan and adjacent regions, central China, *Int. Geol. Rev.*, *37*(8), 661–735.

Burov, E. B. (2011), Rheology and strength of the lithosphere, *Mar. Petrol. Geol.*, *28*(8), 1402–1443.

Burov, E. B., and M. Diament (1995), The effective elastic thickness (Te) of continental lithosphere: What does it really mean?, *J. Geophys. Res.*, *100*, 3905–3905, doi:10.1029/3994JB02770.

Byerlee, J. (1978), Friction of rocks, *Pure Appl. Geophys.*, *116*(4–5), 615–626.

Cammarano, F., S. Goes, P. Vacher, and D. Giardini (2003), Inferring upper-mantle temperatures from seismic velocities, *Phys. Earth Planet. Inter.*, *138*(3), 197–222.

Carter, N. L., and M. C. Tsenn (1987), Flow properties of continental lithosphere, *Tectonophysics*, *136*(1), 27–63.

Chen, L., W. Tao, L. Zhao, and T. Zheng (2008), Distinct lateral variation of lithospheric thickness in the Northeastern North China Craton, *Earth Planet. Sci. Lett.*, *267*(1–2), 56–68, doi:10.1016/j.epsl.2007.11.024.

Chen, L., C. Cheng, and Z. Wei (2009), Seismic evidence for significant lateral variations in lithospheric thickness beneath the central and western North China craton, *Earth Planet. Sci. Lett.*, *286*(1), 171–183.

Chen, L., F. Berntsson, Z. Zhang, P. Wang, J. Wu, and T. Xu (2014), Seismically constrained thermo-rheological structure of the eastern Tibetan margin: Implication for lithospheric delamination, *Tectonophysics*, *627*, 122–134.

Chen, Y., W. Li, X. Yuan, J. Badal, and J. Teng (2015), Tearing of the Indian lithospheric slab beneath southern Tibet revealed by *SKS*-wave splitting measurements, *Earth Planet. Sci. Lett.*, *413*, 13–24.

Clark, M. K., and L. H. Royden (2000), Topographic ooze: Building the eastern margin of Tibet by lower crustal flow, *Geology*, *28*(8), 703–706.

Copley, A., J. P. Avouac, and J. Y. Royer (2010), India-Asia collision and the Cenozoic slowdown of the Indian plate: Implications for the forces driving plate motions, *J. Geophys. Res.*, *115*, B03410, doi:10.1029/2009JB006634.

Craig, T. J., A. Copley, and J. Jackson (2012), Thermal and tectonic consequences of India underthrusting Tibet, *Earth Planet. Sci. Lett.*, *353*, 231–239.

Deichmann, N. (1992), Structural and rheological implications of lower-crustal earthquakes below northern Switzerland, *Phys. Earth Planet. Inter.*, *69*(3), 270–280.

Demouchy, S., A. Tommasi, T. Boffa Ballaran, and P. Cordier (2013), Low strength of Earth's uppermost mantle inferred from tri-axial deformation experiments on dry olivine crystals, *Phys. Earth Planet. Int.*, *220*, 37–49.

Deng, Y., W. Shen, T. Xu, and M. H. Ritzwoller (2015), Crustal layering in northeastern Tibet: A case study based on joint inversion of receiver functions and surface wave dispersion, *Geophys. J. Int.*, *203*, 692–706.

Dong, Z., J. Tang, M. Unsworth, and X. Chen (2015), Electrical resistivity structure of the upper mantle beneath Northeastern China: Implications for rheology and the mechanism of craton destruction, *J. Asian Earth Sci.*, *100*, 115–131.

England, P. C., R. T. Walker, B. Fu, and M. A. Floyd (2013), A bound on the viscosity of the Tibetan crust from the horizontality of palaeolake shorelines, *Earth Planet. Sci. Lett.*, *375*, 44–56, doi:10.1016/j.epsl.2013.05.001.

England, P., and P. Molnar (1997), Active deformation of Asia: From kinematics to dynamics, *Science*, *278*, 647–650.

Enkelmann, E., L. Ratschbacher, R. Jonckheere, R. Nestler, M. Fleischer, R. Gloaguen, B. R. Hacker, Y. Q. Zhang, and Y.-S. Ma (2006), Cenozoic exhumation and deformation of northeastern Tibet and the Qinling: Is Tibetan lower crustal flow diverging around the Sichuan Basin?, *Geol. Soc. Am. Bull.*, *118*(5–6), 651–671.

Evans, B., and C. Goetze (1979), The temperature variation of hardness of olivine and its implication for polycrystalline yield stress, *J. Geophys. Res.*, *84*, 5505–5524, doi:10.1029/JB084iB10p05505.

Fan, W. M., H. F. Zhang, J. Baker, K. E. Jarvis, P. R. D. Mason, and M. A. Menzies (2000), On and off the North China Craton: Where is the Archaean keel?, *J. Petrol.*, *41*(7), 933–950.

Feng, C., S. Liu, L. Wang, and C. Li (2009), Present-day geothermal regime in Tarim Basin, Northwest China, *Chinese J. Geophys.*, *52*(6), 1237–1250.
Feng, M., S. van der Lee, M. An, and Y. Zhao (2010), Lithospheric thickness, thinning, subduction, and interaction with the asthenosphere beneath China from the joint inversion of seismic *S*-wave train fits and Rayleigh-wave dispersion curves, *Lithos*, *120*(1), 116–130.
Flesch, L. M., A. J. Haines, and W. E. Holt (2001), Dynamics of the India-Eurasia collision zone, *J. Geophys. Res.*, *106*, 16,435–16,460, doi:10.1029/2001JB000208.
Flesch, L. M., W. E. Holt, P. G. Silver, M. Stephenson, C.-Y. Wang, and W. W. Chan (2005), Constraining the extent of crust–mantle coupling in central Asia using GPS, geologic, and shear wave splitting data, *Earth Planet. Sci. Lett.*, *238*(1), 248–268.
François, T., E. Burov, B. Meyer, and P. Agard (2013), Surface topography as key constraint on thermo-rheological structure of stable cratons, *Tectonophysics*, *602*, 106–123.
Fu, S. F., and B. C. Liu (1980), *Seismology*, Beijing Univ. Press, Beijing.
Gan, W., P. Zhang, Z. K. Shen, Z. Niu, M. Wang, Y. Wan, D. Zhou, and J. Cheng (2007), Present-day crustal motion within the Tibetan Plateau inferred from GPS measurements, *J. Geophys. Res.*, *112*, B08416, doi:10.1029/2005JB004120.
Goetze, C., and B. Evans (1979), Stress and temperature in the bending lithosphere as constrained by experimental rock mechanics, *Geophys. J. Int.*, *59*(3), 463–478.
Griffin, W., Z. Andi, S. O'reilly, and C. Ryan (1998), Phanerozoic evolution of the lithosphere beneath the Sino-Korean Craton, *Geodyn. Ser.*, *27*, 107–126.
Griffin, W., S. O'Reilly, N. Abe, S. Aulbach, R. Davies, N. Pearson, B. Doyle, and K. Kivi (2003), The origin and evolution of Archean lithospheric mantle, *Precambrian Res.*, *127*(1–3), 19–41.
Gutenberg, B., and C. F. Richter (1956), Magnitude and energy of earthquakes, *Ann. Geophys.*, *9*(1), 1–15.
Hacker, B. R., E. Gnos, L. Ratschbacher, M. Grove, M. McWilliams, S. V. Sobolev, J. Wan, and W. Zhenhan (2000), Hot and dry deep crustal xenoliths from Tibet, *Science*, *287*, 2463–2466.
Hirn, A., M. Jiang, M. Sapin, J. Diaz, A. Nercessian, Q. Lu, J. Lepine, D. Shi, M. Sachpazi, and M. Pandey (1995), Seismic anisotropy as an indicator of mantle flow beneath the Himalayas and Tibet, *Nature*, *375*(6532), 571–574.
Hirth, G., and D. L. Kohlstedt (1996), Water in the oceanic upper mantle: Implications for rheology, melt extraction and the evolution of the lithosphere, *Earth Planet. Sci. Lett.*, *144*(1), 93–108.
Hu, S., L. He, and J. Wang (2000), Heat flow in the continental area of China: A new data set, *Earth Planet. Sci. Lett.*, *179*(2), 407–419.
Huang, M.-H., R. Bürgmann, and A. M. Freed (2014), Probing the lithospheric rheology across the eastern margin of the Tibetan Plateau, *Earth Planet. Sci. Lett.*, *396*, 88–96.
Huang, Z., M. Xu, L. Wang, N. Mi, D. Yu, and H. Li (2008), Shear wave splitting in the southern margin of the Ordos Block, north China, *Geophys. Res. Lett.*, *35*, L19301, doi:10.1029/2008GL035188.
Jackson, I., and S. M. Rigden (1996), Analysis of P-V-T data: Constraints on the thermoelastic properties of high-pressure minerals, *Phys. Earth Planet. Int.*, *96*, 85–112.
Jackson, I., F. Gerald, D. John, U. H. Faul, and B. H. Tan (2002), Grain-size-sensitive seismic wave attenuation in polycrystalline olivine, *J. Geophys. Res.*, *107*(B12), 2360, doi:10.1029/2001JB001225.
Jackson, J. (2002), Strength of the continental lithosphere: Time to abandon the jelly sandwich?, *GSA Today*, *12*(9), 4–9.
Ji, S., Q. Wang, and M. H. Salisbury (2009), Composition and tectonic evolution of the Chinese continental crust constrained by Poisson's ratio, *Tectonophysics*, *463*(1), 15–30.
Jiang, C., Y. Yang, and Y. Zheng (2014), Penetration of mid-crustal low velocity zone across the Kunlun Fault in the NE Tibetan Plateau revealed by ambient noise tomography, *Earth Planet. Sci. Lett.*, *406*, 81–92.
Jiménez-Diaz, A., J. Ruiza, M. Pérez-Gussinye, J. F. Kirby, J. A. Alvarez-Gomez, R. Tejero, and R. Capote (2014), Spatial variations of effective elastic thickness of the lithosphere in Central America and surrounding regions, *Earth Planet. Sci. Lett.*, *391*, 55–66.
Jiménez-Munt, I., M. Fernàndez, J. Vergés, and J. P. Platt (2008), Lithosphere structure underneath the Tibetan Plateau inferred from elevation, gravity and geoid anomalies, *Earth Planet. Sci. Lett.*, *267*, 276–289.
Karato, S., and H. Spetzler (1990), Defect microdynamics in minerals and solid-state mechanisms of seismic wave attenuation and velocity dispersion in the mantle, *Rev. Geophys.*, *28*, 399–421, doi:10.1029/RG028i004p00399.
Karplus, M., W. Zhao, S. Klemperer, Z. Wu, J. Mechie, D. Shi, L. Brown, and C. Chen (2011), Injection of Tibetan crust beneath the south Qaidam Basin: Evidence from INDEPTH IV wide-angle seismic data, *J. Geophys. Res.*, *116*, B07301, doi:10.1029/2010JB007911.
Karplus, M., S. Klemperer, J. Lawrence, W. Zhao, J. Mechie, F. Tilmann, E. Sandvol, and J. Ni (2013), Ambient-noise tomography of north Tibet limits geological terrane signature to upper-middle crust, *Geophys. Res. Lett.*, *40*, 808–813, doi:10.1002/grl.50202.
Kirby, S. H. (1983), Rheology of the lithosphere, *Rev. Geophys.*, *21*, 1458–1487, doi:10.1029/RG021i006p01458.
Klemperer, S. L. (2006), Crustal flow in Tibet: Geophysical evidence for the physical state of Tibetan lithosphere, and inferred patterns of active flow, *Geol. Soc. London, Special Publications*, *268*(1), 39–70.
Koulakov, I. (2011), High-frequency *P* and *S* velocity anomalies in the upper mantle beneath Asia from inversion of worldwide traveltime data, *J. Geophys. Res.*, *116*, B04301, doi:10.1029/2010JB007938.
Kreemer, C., G. Blewitt, and E. C. Klein (2014), A geodetic plate motion and global strain rate model, *Geochem. Geophys. Geosyst.*, *15*, 3849–3889, doi:10.1002/2014GC005407.
Kumar, P., X. Yuan, R. Kind, and G. Kosarev (2005), The lithosphere-asthenosphere boundary in the Tien Shan-Karakoram region from S receiver functions: Evidence for continental subduction, *Geophys. Res. Lett.*, *32*, L07305, doi:10.1029/2004GL022291.
Laske, G., G. Masters, Z. Ma, and M. Pasyanos (2013), Update on CRUST1. 0-A 1-degree global model of Earth's crust, paper presented at Geophys. Res. Abstracts.
Li, Y., Q. Wu, F. Zhang, Q. Feng, and R. Zhang (2011), Seismic anisotropy of the Northeastern Tibetan Plateau from shear wave splitting analysis, *Earth Planet. Sci. Lett.*, *304*(1), 147–157.
Li, Y., Q. Wu, J. Pan, F. Zhang, and D. Yu (2013), An upper-mantle *S*-wave velocity model for East Asia from Rayleigh wave tomography, *Earth Planet. Sci. Lett.*, *377*, 367–377.
Li, Y., Q. Wu, R. Zhang, X. Tian, and R. Zeng (2008), The crust and upper mantle structure beneath Yunnan from joint inversion of receiver functions and Rayleigh wave dispersion data, *Phys. Earth Planet. Inter.*, *170*(1), 134–146.
Li, Z. X., and X. H. Li (2007), Formation of the 1300-km-wide intracontinental orogen and postorogenic magmatic province in Mesozoic South China: A flat-slab subduction model, *Geology*, *35*(2), 179–182.
Li, Z., S. Ni, and S. Roecker (2014), Interstation Pg and Sg differential traveltime tomography in the northeastern margin of the Tibetan Plateau: Implications for spatial extent of crustal flow and segmentation of the Longmenshan fault zone, *Phys. Earth Planet. Inter.*, *227*, 30–40.

Liu, M., X. Cui, and F. Liu (2004), Cenozoic rifting and volcanism in eastern China: A mantle dynamic link to the Indo–Asian collision?, *Tectonophysics*, *393*(1), 29–42.
Lund, M. G., H. Austrheim, and M. Erambert (2004), Earthquakes in the deep continental crust-insights from studies on exhumed high-pressure rocks, *Geophys. J. Int.*, *158*(2), 569–576.
Maggi, A., J. Jackson, D. McKenzie, and K. Priestley (2000), Earthquake focal depths, effective elastic thickness, and the strength of the continental lithosphere, *Geology*, *28*(6), 495.
Mareschal, J.-C., and C. Jaupart (2013), Radiogenic heat production, thermal regime and evolution of continental crust, *Tectonophysics*, *609*, 524–534.
McDonough, W. F., and S.-S. Sun (1995), The composition of the Earth, *Chem. Geol.*, *120*(3), 223–253.
McKenzie, D., and K. Priestley (2008), The influence of lithospheric thickness variations on continental evolution, *Lithos*, *102*(1), 1–11.
Mei, S., A. Suzuki, D. L. Kohlstedt, N. A. Dixon, and W. B. Durham (2010), Experimental constraints on the strength of the lithospheric mantle, *J. Geophys. Res.*, *115*, B08204, doi:10.1029/2009JB006873.
Menzies, M., Y. Xu, H. Zhang, and W. Fan (2007), Integration of geology, geophysics and geochemistry: A key to understanding the North China Craton, *Lithos*, *96*(1), 1–21.
Nunn, C., S. W. Roecker, F. J. Tilmann, K. F. Priestley, R. Heyburn, E. A. Sandvol, J. F. Ni, Y. J. Chen, W. Zhao, and I. Team (2014), Imaging the lithosphere beneath NE Tibet: Teleseismic P and S body wave tomography incorporating surface wave starting models, *Geophys. J. Int.*, *196*(3), 1724–1741.
Pandey, S., X. Yuan, E. Debayle, K. Priestley, R. Kind, F. Tilmann, and X. Li (2014), A 3D shear-wave velocity model of the upper mantle beneath China and the surrounding areas, *Tectonophysics*, *633*, 193–210.
Panza, G., and R. Raykova (2008), Structure and rheology of lithosphere in Italy and surrounding, *Terra Nova*, *20*(3), 194–199.
Pollack, H. N., and D. S. Chapman (1977), On the regional variation of heat flow, geotherms, and lithospheric thickness, *Tectonophysics*, *38*(3), 279–296.
Priestley, K., and D. McKenzie (2006), The thermal structure of the lithosphere from shear wave velocities, *Earth Planet. Sci. Lett.*, *244*(1), 285–301.
Qiu, R. Z., T. D. Li, J. F. Deng, S. Zhou, Q. Xiao, T. Ye, S. Geng, X. Cheng, C. Wang, and Y. Liu (2006), Large-scale metallogenesis and petroleum field formation in continental China-constraints from the lithosphere, *Geol. China*, *33*(4), 852–865.
Ranalli, G. (1994), Nonlinear flexure and equivalent mechanical thickness of the lithosphere, *Tectonophysics*, *240*(1), 107–114.
Ranalli, G. (1995), *Rheology of the Earth*, Springer, London.
Ranalli, G., and D. C. Murphy (1987), Rheological stratification of the lithosphere, *Tectonophysics*, *132*(4), 281–295.
Ranalli, G., and M. Adams (2013), Rheological contrast at the continental Moho: Effects of composition, temperature, deformation mechanism, and tectonic regime, *Tectonophysics*, *609*, 480–490.
Robert, A. M. M., M. Fernandez, I. Jimenez-Munt, and J. Verges (2015), *Lithospheric Structure in Central Eurasia Derived From Elevation, Geoid Anomaly and Thermal Analysis*, *Special Publications*, vol. 427, Geol. Soc., London, doi:10.1144/SP427.10.
Royden, L. H., B. C. Burchfiel, and R. D. van der Hilst (2008), The geological evolution of the Tibetan Plateau, *Science*, *321*(5892), 1054–1058.
Sato, H., I. S. Sacks, T. Murase, G. Muncill, and H. Fukuyama (1989), Qp-melting temperature relation in peridotite at high pressure and temperature: Attenuation mechanism and implications for the mechanical properties of the upper mantle, *J. Geophys. Res.*, *94*, 10,647–10,661, doi:10.1029/JB094iB08p10647.
Simmons, N. A., S. C. Myers, G. Johannesson, and E. Matzel (2012), LLNL-G3Dv3: Global *P* wave tomography model for improved regional and teleseismic travel time prediction, *J. Geophys. Res.*, *117*, B10302, doi:10.1029/2012JB009525.
Singh, A., C. Singh, and B. Kennett (2015), A review of crust and upper mantle structure beneath the Indian subcontinent, *Tectonophysics*, *644*, 1–21.
Sloan, R., J. Jackson, D. McKenzie, and K. Priestley (2011), Earthquake depth distributions in central Asia, and their relations with lithosphere thickness, shortening and extension, *Geophys. J. Int.*, *185*(1), 1–29.
Spinelli, G. A., and K. Wang (2008), Effects of fluid circulation in subducting crust on Nankai margin seismogenic zone temperatures, *Geology*, *36*(11), 887–890.
Stixrude, L., and C. Lithgow-Bertelloni (2005), Thermodynamics of mantle minerals—I. Physical properties, *Geophys. J. Int.*, *162*(2), 610–632.
Sun, X., X. Song, S. Zheng, Y. Yang, and M. H. Ritzwoller (2010), Three dimensional shear wave velocity structure of the crust and upper mantle beneath China from ambient noise surface wave tomography, *Earthquake. Sci.*, *23*(5), 449–463.
Sun, Y., S. Dong, H. Zhang, H. Li, and Y. Shi (2013a), 3D thermal structure of the continental lithosphere beneath China and adjacent regions, *J. Asian Earth Sci.*, *62*, 697–704.
Sun, Y., S. Dong, H. Zhang, and Y. Shi (2014), Numerical investigation of the geodynamic mechanism for the late Jurassic deformation of the Ordos block and surrounding orogenic belts, *J. Asian Earth Sci.*, doi:10.1016/j.jseaes.2014.08.033.
Sun, Y.-J., S.-W. Dong, T.-Y. Fan, H. Zhang, and Y.-L. Shi (2013b), 3D rheological structure of the continental lithosphere beneath China and adjacent regions, *Chinese J. Geophys.*, *56*(5), 546–558.
Tesauro, M., M. K. Kaban, and S. A. P. L. Cloetingh (2012), Global strength and elastic thickness of the lithosphere, *Global Planet. Change*, *90–91*, 51–57.
Tesauro, M., M. K. Kaban, and S. A. P. L. Cloetingh (2013), Global model for the lithospheric strength and effective elastic thickness, *Tectonophysics*, *602*, 78–86.
Tesauro, M., M. K. Kaban, W. D. Mooney, and S. A. P. L. Cloetingh (2014), Density, temperature and composition of the North American lithosphere: New insights form a joint analysis of seismic, gravity and mineral physics data. Part II: Thermal and compositional model of the upper mantle, *Geophys. Geochem. Geosyst.*, *15*, 4808–4830, doi:10.1002/2014GC005484.
Tesauro, M., M. K. Kaban, and W. D. Mooney (2015), Variations of the lithospheric strength and elastic thickness in North America, *Geochem. Geophys. Geosyst*, *16*, 2197–2220, doi:10.1002/2015GC005937.
Tian, X., D. Zhao, H. Zhang, Y. Tian, and Z. Zhang (2010), Mantle transition zone topography and structure beneath the central Tien Shan orogenic belt, *J. Geophys. Res.*, *115*, B10308, doi:10.1029/2008JB006229.
Tunini, L., I. Jiménez-Munt, M. Fernandez, J. Vergés, A. Villaseñor, M. Melchiorre, and J.-C. Afonso (2016), Geophysical-petrological model of the crust and upper mantle in the India-Eurasia collision zone, *Tectonics*, *35*, 1642–1669, doi:10.1002/2016TC004161.
Wang, C.-Y., L. M. Flesch, P. G. Silver, L.-J. Chang, and W. W. Chan (2008), Evidence for mechanically coupled lithosphere in central Asia and resulting implications, *Geology*, *36*(5), 363–366.
Wang, C.-Y., W.-P. Chen, and L.-P. Wang (2013a), Temperature beneath Tibet, *Earth Planet. Sci. Lett.*, *375*, 326–337.
Wang, C.-Y., E. Sandvol, L. Zhu, H. Lou, Z. Yao, and X. Luo (2014), Lateral variation of crustal structure in the Ordos block and surrounding regions, North China, and its tectonic implications, *Earth Planet. Sci. Lett.*, *387*, 198–211.

Wang, Q., S.-L. Chung, X.-H. Li, D. Wyman, Z.-X. Li, W.-D. Sun, H.-N. Qiu, Y.-S. Liu, and Y.-T. Zhu (2012), Crustal melting and flow beneath Northern Tibet: Evidence from Mid-Miocene to Quaternary strongly peraluminous rhyolites in the Southern Kunlun Range, *J. Petrol.*, *53*, 2523–2566.

Wang, R., D. Zhou, J. Wang, Y. Wang, and Y. Liu (1999), Variscan terrane of deep-crustal granulite facies in Yushugou area, southern Tianshan, *Sci. China Earth Sci.*, *42*(5), 482–490.

Wang, Y., and S. Cheng (2012), Lithospheric thermal structure and rheology of the eastern China, *J. Asian Earth Sci.*, *47*, 51–63.

Wang, Y., W. D. Mooney, X. Yuan, and N. Okaya (2013b), Crustal structure of the Northeastern Tibetan Plateau from the southern Tarim basin to the Sichuan Basin, China, *Tectonophysics*, *584*, 191–208.

Wei, W., J. Xu, D. Zhao, and Y. Shi (2012), East Asia mantle tomography: New insight into plate subduction and intraplate volcanism, *J. Asian Earth Sci.*, *60*, 88–103, doi:10.1016/j.jseaes.2012.08.001.

Wei, W., M. Unsworth, A. Jones, J. Booker, H. Tan, D. Nelson, L. Chen, S. Li, K. Solon, and P. Bedrosian (2001), Detection of widespread fluids in the Tibetan crust by magnetotelluric studies, *Science*, *292*(5517), 716-719.

Wei, W., et al. (2014), Northward channel flow in northern Tibet revealed from 3D magnetotelluric modelling, *Phys. Earth Planet. Inter.*, *235*, 13–24.

Wilks, K. R., and N. L. Carter (1990), Rheology of some continental lower crustal rocks, *Tectonophysics*, *182*(1), 57–77.

Windley, B. F., S. Maruyama, and W. J. Xiao (2010), Delamination/thinning of sub-continental lithospheric mantle under Eastern China: The role of water and multiple subduction, *Am. J. Sci.*, *310*(10), 1250–1293, doi:10.2475/10.2010.03.

Xiao, Q., J. Zhang, G. Zhao, and J. Wang (2013), Electrical resistivity structures northeast of the Eastern Kunlun Fault in the Northeastern Tibet: Tectonic implications, *Tectonophysics*, *601*, 125–138.

Xie, J., M. H. Ritzwoller, W. Shen, Y. Yang, Y. Zheng, and L. Zhou (2013), Crustal radial anisotropy across eastern Tibet and the western Yangtze craton, *J. Geophys. Res. Solid Earth*, *118*, 4226–4252, doi:10.1002/jgrb.50296.

Xu, C. (2003), The study of lithospheric tectonics and basin formation of Chinese mainland and migration of oil and gas, *Earth Sci. Front.*, *10*(3), 113–127.

Xu, T., Z. Wu, Z. Zhang, X. Tian, Y. Deng, C. Wu, and J. Teng (2014), Crustal structure across the Kunlun fault from passive source seismic profiling in East Tibet, *Tectonophysics*, *627*, 98–107.

Xu, Y.-G. (2007), Diachronous lithospheric thinning of the North China Craton and formation of the Daxin'anling–Taihangshan gravity lineament, *Lithos*, *96*(1–2), 281–298, doi:10.1016/j.lithos.2006.09.013.

Yang, Y., M. H. Ritzwoller, Y. Zheng, W. Shen, A. L. Levshin, and Z. Xie (2012), A synoptic view of the distribution and connectivity of the mid-crustal low velocity zone beneath Tibet, *J. Geophys. Res.*, *117*, B04303, doi:10.1029/2011JB008810.

Yang, S., X. Xiong, Y. Zheng, and B. Shan (2013), Upper-mantle temperature and lithospheric thickness of North China, *Chinese J. Geophys.*, *56*(11), 3855–3867.

Zhang, C.-L., H.-B. Zou, H.-K. Li, and H.-Y. Wang (2013a), Tectonic framework and evolution of the Tarim Block in NW China, *Gondwana Res.*, *23*, 1306–1315, doi:10.1016/j.gr.2012.05.009.

Zhang, H., J. Teng, X. Tian, Z. Zhang, R. Gao, and J. Liu (2012), Lithospheric thickness and upper-mantle deformation beneath the NE Tibetan Plateau inferred from *S* receiver functions and *SKS* splitting measurements, *Geophys. J. Int.*, *191*(3), 1285–1294, doi:10.1111/j.1365-246X.2012.05667.x.

Zhang, Z., X. Yuan, Y. Chen, X. Tian, R. Kind, X. Li, and J. Teng (2010), Seismic signature of the collision between the east Tibetan escape flow and the Sichuan Basin, *Earth Planet. Sci. Lett.*, *292*(3–4), 254–264.

Zhang, Z., Q. Chen, Z. Bai, Y. Chen, and J. Badal (2011a), Crustal structure and extensional deformation of thinned lithosphere in Northern China, *Tectonophysics*, *508*(1–4), 62–72, doi:10.1016/j.tecto.2010.06.021.

Zhang, Z., L. Yang, J. Teng, and J. Badal (2011b), An overview of the earth crust under China, *Earth Sci. Rev.*, *104*(1–3), 143–166, doi:10.1016/j.earscirev.2010.10.003.

Zhang, Z., Y. Deng, L. Chen, J. Wu, J. Teng, and G. Panza (2013b), Seismic structure and rheology of the crust under mainland China, *Gondwana Res.*, *23*(4), 1455–1483, doi:10.1016/j.gr.2012.07.010.

Zhang, Z., J. Teng, F. Romanelli, C. Braitenberg, Z. Ding, X. Zhang, L. Fang, S. Zhang, J. Wu, and Y. Deng (2014), Geophysical constraints on the link between cratonization and orogeny: Evidence from the Tibetan Plateau and the North China Craton, *Earth Sci. Rev.*, *130*, 1–48.

Zhao, L., X. Xie, J. He, X. Tian, and Z. Yao (2013), Crustal flow pattern beneath the Tibetan Plateau constrained by regional Lg-wave Q tomography, *Earth Planet. Sci. Lett.*, *383*, 113–122.

Zheng, J., W. Griffin, S. Y. O'Reilly, C. Yu, H. Zhang, N. Pearson, and M. Zhang (2007), Mechanism and timing of lithospheric modification and replacement beneath the eastern North China Craton: Peridotitic xenoliths from the 100 Ma Fuxin basalts and a regional synthesis, *Geochim. Cosmochim. Acta*, *71*(21), 5203–5225.

Zheng, S., X. Sun, X. Song, Y. Yang, and M. H. Ritzwoller (2008), Surface wave tomography of China from ambient seismic noise correlation, *Geochem. Geophys. Geosyst.*, *9*, Q05020, doi:10.1029/2008GC001981.

Zheng, T.-Y., L. Zhao, Y.-M. He, and R.-X. Zhu (2014), Seismic imaging of crustal reworking and lithospheric modification in eastern China, *Geophys. J. Int.*, *196*, 657–670, doi:10.1093/gji/ggt420.

Zheng, Y.-F., W.-J. Xiao, and G. Zhao (2013), Introduction to tectonics of China, *Gondwana Res.*, *23*(4), 1189–1206, doi:10.1016/j.gr.2012.10.001.

Zhou, H., and M. A. Murphy (2005), Tomographic evidence for wholesale underthrusting of India beneath the entire Tibetan Plateau, *J. Asian Earth Sci.*, *25*(3), 445–457.

Zhu, G., D. Jiang, B. Zhang, and Y. Chen (2012), Destruction of the eastern North China Craton in a backarc setting: Evidence from crustal deformation kinematics, *Gondwana Res.*, *22*(1), 86–103.

Zhu, R., L. Chen, F. Wu, and J. Liu (2011), Timing, scale and mechanism of the destruction of the North China Craton, *Sci. China Earth Sci.*, *54*(6), 789–797, doi:10.1007/s11430-011-4203-4.

Zhu, S., and Y. Shi (2011), Estimation of GPS strain rate and its error analysis in the Chinese continent, *J. Asian Earth Sci.*, *40*, 351–362.